Hindawi
Shock and Vibration
Volume 2020, Article ID 8830460, 24 pages
https://doi.org/10.1155/2020/8830460

Research Article

Multihazard Response Control of Base-Isolated Buildings under Bidirectional Dynamic Excitation

Daniel H. Zelleke,[1] **Sandip K. Saha**,[2] **and Vasant A. Matsagar**[1]

[1]*Multi-Hazard Protective Structures (MHPS) Laboratory, Department of Civil Engineering, Indian Institute of Technology (IIT) Delhi, Hauz Khas, New Delhi 110016, India*
[2]*School of Engineering, Indian Institute of Technology (IIT) Mandi, Kamand, Mandi 175005, India*

Correspondence should be addressed to Vasant A. Matsagar; matsagar@civil.iitd.ac.in

Received 21 June 2020; Revised 7 September 2020; Accepted 4 November 2020; Published 21 December 2020

Academic Editor: Franck Poisson

The issues of safety and posthazard functionality of structures under multihazard scenarios are some of the significant challenges in the current dynamic and rapidly growing urban environment. In this paper, multistory base-isolated buildings are investigated under the independent multihazard scenario of earthquake and blast-induced ground motion (BIGM). Multistory building models equipped with five different types of isolation systems, namely, the laminated rubber bearing (LRB), lead-rubber bearing (N-Z system), pure friction (PF) system, friction pendulum system (FPS), and resilient-friction base isolator (R-FBI) are assessed under bidirectional multihazard excitations. The suitability of the isolation systems and their key parameters in protecting multistory buildings is evaluated. Furthermore, the influence of the superstructure characteristics, such as the superstructure damping and the number of stories, is also assessed. The effect of bidirectional hazards on fixed-base buildings is also presented for comparison. The key response quantities of base-isolated buildings are presented and compared for different isolation systems. Parametric investigations are also conducted, and the trends of the response quantities are presented to study the influence of important parameters of isolation systems in protecting the buildings under the multihazard scenario of earthquake and BIGM. The results of the investigation show that the behaviors of the buildings equipped with various isolation systems are different for the two hazards. Moreover, the influences of the key parameters of the isolation systems are found to be different for various hazards. Therefore, the selection of design parameters of isolation systems shall be made with due consideration of the influence of multiple hazards. Additionally, the influence of the properties of the superstructure, such as the number of stories and the damping of the superstructure, on the behavior of the base-isolated buildings under the multihazard loading, is presented.

1. Introduction

Earthquakes have been and remain to be one of the prominent threats to the safety and serviceability of civil engineering structures and infrastructure systems. Numerous strategies have been proposed, researched, and implemented for seismic protection of structures [1–4]. The use of structural response control strategies has been proven to be an effective approach. Base isolation is an effective strategy to protect structures, the inhabitants of the structures, and the contents housed within the structures against the undesirable effects of earthquakes. It reduces the earthquake force imparted on the superstructure by increasing the fundamental time period of the structure and dissipating the earthquake energy [5, 6]. Various types of base isolation strategies, such as the elastomeric type bearings, sliding bearings, and rolling bearings, have been proposed [6]. Also, different active and semiactive seismic isolation strategies have attracted researchers' attention in recent years [7–10].

Structures, including those equipped with base isolation systems, are also likely to be subjected to other hazards in their service life, which necessitates the consideration of various types of loadings in the design of structures. Despite the significant socioeconomic impact caused by various natural and human-made hazards [11, 12], such as blast, impact, earthquake, tsunami, and wind, less attention is

devoted on research and development to understand the behavior of structures under multiple hazards and to devise design strategies thereof. Additionally, the risk associated with the reduced safety and serviceability of key infrastructures, categorized as lifeline structures, such as hospitals, bridges, power plants, data centers, and communication centers, is paramount. Therefore, it is crucial to design structures, especially the critical infrastructures, by considering all the hazards likely to affect safety and serviceability. There is limited research on the use of the multihazard approach in the performance assessment and design of structures. For instance, Messervey et al. [13], Gardoni and LaFave [12], Mahmoud and Chulahwat [14], Venanzi et al. [15], and Roy and Matsagar [16, 17] have conducted studies on the multihazard protection of structures.

Although base isolation is an effective strategy to mitigate the adverse effects of earthquakes, its efficacy in protecting structures under multihazard loading is not explored adequately. Most of the studies on the base-isolated structures also focus on earthquake protection, and therefore, there are limited studies that are conducted on the performance assessment of base-isolated structures under other hazards, such as wind and blast. Some of the attempts to investigate the behavior of base-isolated structures under wind loading include the studies conducted by Henderson and Novak [18, 19]. They have conducted theoretical and experimental studies to assess the response of the base-isolated buildings under wind loading, wherein the theoretical and experimental results are compared. Chen and Ahmadi [20] have evaluated the sensitivity of structures isolated by the laminated rubber bearing (LRB), high damping rubber bearing (HDRB), and resilient-rubber bearing (R-FBI) to wind loading. Furthermore, Kareem [21] has studied the dynamic response of base-isolated buildings with passive dampers under wind loading. Later, Liang et al. [22] have assessed the habitability of base-isolated buildings under fluctuating wind load. Recently, a probabilistic investigation on the response of tall base-isolated buildings under wind loading has been reported by Feng and Chen [23].

The response of base-isolated structures under surface blast has been assessed by some researchers. Zhang and Phillips [24, 25] have studied the performance of a multistory base-isolated building with and without passive supplemental dampers in suppressing the vibration response of the building exposed to blast loading. Also, Kangda and Bakre [26] have assessed the response of base-isolated structures subjected to surface blast and concluded that base isolation could be effective in mitigating the blast response quantities, such as the peak story displacement, story drift, and root mean square (RMS) absolute acceleration. The performance of base-isolated buildings under blast-induced ground motion (BIGM) has also captured attention in the recent times. Mondal et al. [27, 28] have studied the response of buildings isolated by lead-rubber bearing (N-Z system) under BIGM. Further, the performance of a base isolation system equipped with shape-memory alloy in protecting buildings under BIGM has been studied by Mondal et al. [29]. Furthermore, the use of various base isolation systems in protecting buildings against blast-induced ground motions has been discussed by Mondal et al. [30]. The findings of the investigations reveal that base isolation can be beneficial to control the vibration response of buildings under blast-induced ground motions. The performance of base isolation strategies for the vibration response control of buildings under other nonseismic hazards, such as train-induced vibrations, has also been explored [31–33]. The available limited literature on the implementation of base isolation for the vibration response control of buildings under different types of excitations indicate the potential benefit of the strategy in mitigating the adverse effects of various types of hazards. Notwithstanding the vibration protection potential of base isolation systems, base-isolated buildings could be influenced differently under distinct types of hazards. Therefore, it is necessary to consider the multihazard approach to satisfy safety and serviceability design requirements for base-isolated buildings that are likely to be subjected to different types of loading. However, there are no studies which investigate the behavior of base-isolated buildings subjected to both earthquakes and blast-induced ground motions. In addition, the influence of the key parameters of the base isolation systems on the efficacy of the response mitigation under the multihazard scenario of earthquake and BIGM has not been explored.

Therefore, it would be essential to investigate and unveil the performance of buildings equipped with the laminated rubber bearing (LRB), lead-rubber bearing (N-Z system), pure friction (PF) system, friction pendulum system (FPS), and resilient-friction base isolator (R-FBI) under the multihazard scenario of earthquake and blast-induced ground motion. Consequently, the behavior of buildings equipped with various base isolation systems is assessed under multihazard loading in this paper. The main objectives of this study include the following: (a) to assess the performance of base-isolated buildings under bidirectional near-fault (NF) earthquake ground motions, far-fault (FF) earthquake ground motions, and blast-induced ground motions (BIGMs), (b) to evaluate the effect of the characteristic parameters of the five base isolation systems, considered herein, on the behavior of base-isolated buildings under different hazards, and (c) to study the effect of the properties of the superstructure on the multihazard response of base-isolated buildings.

2. Modeling of a Base-Isolated Building under Bidirectional Excitation

The schematic diagram and idealized model of the base-isolated building considered in this investigation are depicted in Figure 1. The three-dimensional model of the base-isolated building portrayed in the figure shows the orientation of the building, the location of the isolators, the superstructure properties, and the base excitation. The mathematical modeling of the base-isolated building

under bidirectional base excitation is described as follows.

2.1. Governing Equations of Motion. The governing equations of motion of the base-isolated building, subjected to ground acceleration, are derived under the assumption that the superstructure remains in the elastic range. Furthermore, it is considered that the floors are infinitely rigid, the beams and columns are axially inextensible, the building is symmetric in both X and Y directions, and the torsional response of the building is neglected. Accordingly, two degrees of freedom, lateral displacements in X and Y directions, at each floor and base mass levels are considered in the formulation of the equations of motion. The matrix form of the governing equations of motion of the base-isolated building under bidirectional base excitation is given as

$$\overline{\mathbf{M}}\ddot{\overline{\mathbf{X}}} + \overline{\mathbf{C}}\dot{\overline{\mathbf{X}}} + \overline{\mathbf{K}}\overline{\mathbf{X}} + \overline{\mathbf{f}} = -\overline{\mathbf{M}}\overline{\mathbf{r}}\ddot{\mathbf{U}}_g, \tag{1}$$

where $\overline{\mathbf{M}}$, $\overline{\mathbf{C}}$, and $\overline{\mathbf{K}}$, respectively, are the mass, damping, and stiffness matrices of the base-isolated building. These structural property matrices are given as

$$\overline{\mathbf{M}} = \begin{bmatrix} m_b & \mathbf{0} & 0 & \mathbf{0} \\ \mathbf{0}^T & \mathbf{M}_s & \mathbf{0}^T & \mathbf{0} \\ 0 & \mathbf{0} & m_b & \mathbf{0} \\ \mathbf{0}^T & \mathbf{0} & \mathbf{0}^T & \mathbf{M}_s \end{bmatrix},$$

$$\overline{\mathbf{C}} = \begin{bmatrix} 0 & c_{1x}\mathbf{r}^b & 0 & \mathbf{0} \\ \mathbf{0}^T & \mathbf{C}_{sx} & \mathbf{0}^T & \mathbf{0} \\ 0 & \mathbf{0} & 0 & c_{1y}\mathbf{r}^b \\ \mathbf{0}^T & \mathbf{0} & \mathbf{0}^T & \mathbf{C}_{sy} \end{bmatrix}, \tag{2}$$

$$\overline{\mathbf{K}} = \begin{bmatrix} 0 & k_{1x}\mathbf{r}^b & 0 & \mathbf{0} \\ \mathbf{0}^T & \mathbf{K}_{sx} & \mathbf{0}^T & \mathbf{0} \\ 0 & \mathbf{0} & 0 & k_{1y}\mathbf{r}^b \\ \mathbf{0}^T & \mathbf{0} & \mathbf{0}^T & \mathbf{K}_{sy} \end{bmatrix},$$

where $\mathbf{M}_s = \text{diag}[m_1, m_2, \ldots, m_j, \ldots, m_N]$ is the superstructure mass matrix of size N; N is the number of stories; m_j is the mass of the j^{th} floor; m_b is the base mass; $\mathbf{C}_{sx}$ and $\mathbf{K}_{sx}$, respectively, are the damping and the stiffness matrices of the superstructure in the X direction; $\mathbf{C}_{sy}$ and $\mathbf{K}_{sy}$, respectively, are the damping and the stiffness matrices of the superstructure in the Y direction; c_{1x} and c_{1y} are the damping constants of the first story of the building in X and Y directions, respectively; k_{1x} and k_{1y} are the stiffnesses of the first story of the building in X and Y directions, respectively; $\mathbf{r}^b = \{1, 0, 0, \ldots, 0\}$ is a row vector of size N; $\mathbf{0} = \{0, 0, \ldots, 0\}$ is a row vector of size N; and $\mathbf{0}$ is a null matrix of size $N \times N$.

Furthermore, the vectors of displacements, velocities, and accelerations of the base-isolated building, $\overline{\mathbf{X}}$, $\dot{\overline{\mathbf{X}}}$, and $\ddot{\overline{\mathbf{X}}}$, respectively, the vector of the restoring forces in the isolator, $\overline{\mathbf{f}}$, the vector of ground accelerations, $\ddot{\mathbf{U}}_g$, and the matrix of influence coefficients, $\overline{\mathbf{r}}$, are given as follows.

$$\begin{aligned} \overline{\mathbf{X}} &= \left\{x_b, \mathbf{X}_s^T, y_b, \mathbf{Y}_s^T\right\}^T, \\ \dot{\overline{\mathbf{X}}} &= \left\{\dot{x}_b, \dot{\mathbf{X}}_s^T, \dot{y}_b, \dot{\mathbf{Y}}_s^T\right\}^T, \\ \ddot{\overline{\mathbf{X}}} &= \left\{\ddot{x}_b, \ddot{\mathbf{X}}_s^T, \ddot{y}_b, \ddot{\mathbf{Y}}_s^T\right\}^T, \\ \overline{\mathbf{f}} &= \left\{-f_{bx}, \mathbf{0}, -f_{by}, \mathbf{0}\right\}^T, \\ \ddot{\mathbf{U}}_g &= \left\{\ddot{x}_g, \left(\ddot{x}_g + \ddot{x}_b\right), \ddot{y}_g, \left(\ddot{y}_g + \ddot{y}_b\right)\right\}^T, \\ \overline{\mathbf{r}} &= \begin{bmatrix} 1 & 0 & 0 & 0 \\ \mathbf{0}^T & \mathbf{r} & \mathbf{0}^T & \mathbf{0}^T \\ 0 & 0 & 1 & 0 \\ \mathbf{0}^T & \mathbf{0}^T & \mathbf{0}^T & \mathbf{r} \end{bmatrix}, \end{aligned} \tag{3}$$

where x_b and y_b, respectively, are the displacements of the base mass relative to the ground in X and Y directions; $\dot{x}_b$ and $\dot{y}_b$, respectively, are the velocities of the base mass relative to the ground in X and Y directions; $\ddot{x}_b$ and $\ddot{y}_b$, respectively, are the accelerations of the base mass relative to the ground in X and Y directions; $\mathbf{X}_s = \{x_1, x_2, \ldots, x_N\}^{\text{T}}$ and $\mathbf{Y}_s = \{y_1, y_2, \ldots, y_N\}^{\text{T}}$, respectively, are the vectors of floor displacements in X and Y directions; $\dot{\mathbf{X}}_s$ and $\dot{\mathbf{Y}}_s$, respectively, are the vectors of floor velocities in X and Y directions; $\ddot{\mathbf{X}}_s$ and $\ddot{\mathbf{Y}}_s$, respectively, are the vectors of floor accelerations in X and Y directions; f_{bx} and f_{by}, respectively, are the X and Y components of the force acting on the base isolators; $\ddot{x}_g$ and $\ddot{y}_g$ are the ground accelerations in X and Y directions, respectively; and $\mathbf{r} = \{1, 1, \ldots, 1\}^T$ is a column vector of influence coefficients of size N. The solution of the governing equations of motion is obtained numerically using state-space formulation.

2.2. Mathematical Modeling of Base Isolators under Bidirectional Excitation. In this study, the multihazard response of multistory buildings isolated by elastomeric and sliding bearings are studied. Two elastomeric bearings, the laminated rubber bearing (LRB) and lead-rubber bearing (N-Z system), are used; whereas, the three types of sliding bearings investigated are the pure friction (PF) system, friction pendulum system (FPS), and resilient-friction base isolator (R-FBI). The mathematical modeling of the base isolation bearings is realized by considering their characteristic parameters. The LRB is mathematically represented using the isolation time period (T_b) and the isolation damping ratio (ξ_b), whereas the N-Z system is modeled using the isolation time period (T_b), the isolation damping ratio (ξ_b), the yield displacement (q), and normalized yield strength (F_0). The PF system is characterized using the friction coefficient (μ_b), and the isolation time period (T_b) and the friction coefficient (μ_b) are used to model the FPS. Furthermore, the isolation time period (T_b), the friction coefficient (μ_b), and the isolation damping ratio (ξ_b) are used to model the R-FBI. The LRB is a linear isolation system, and the restoring forces of the bearing in X and Y directions can be obtained as

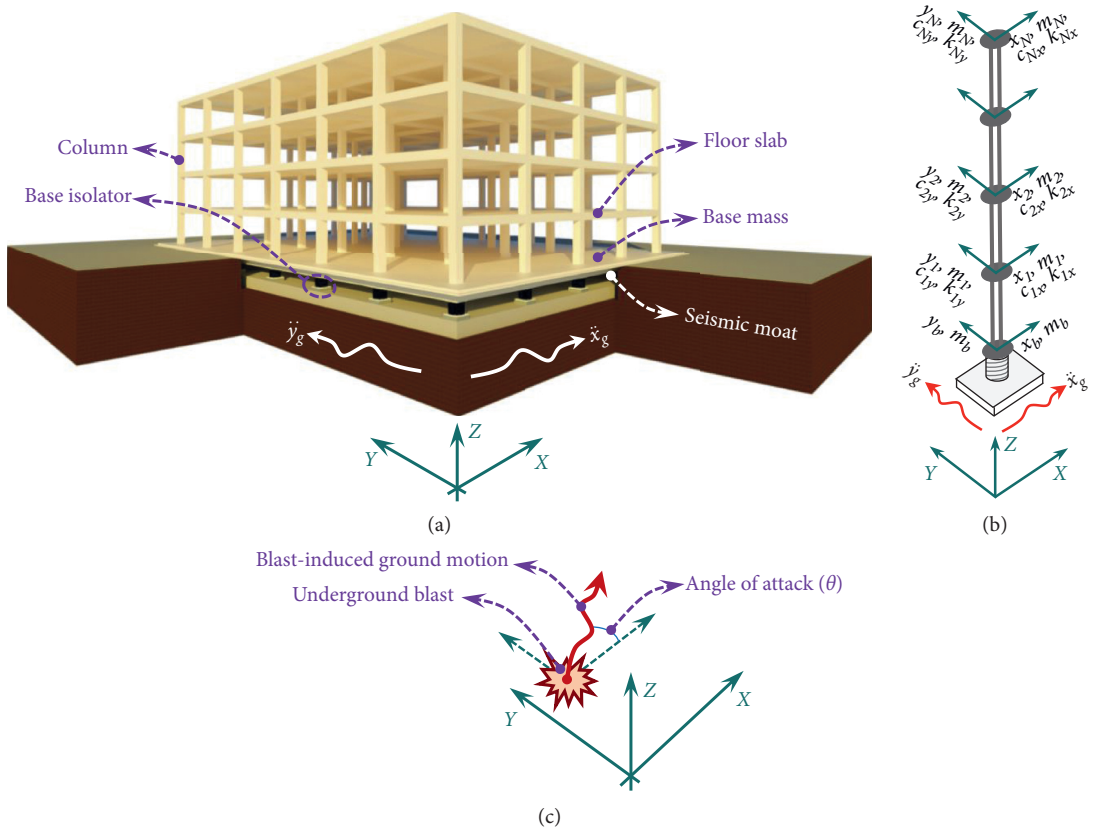

FIGURE 1: Base-isolated building subjected to bidirectional base excitation: (a) schematic diagram, (b) idealized model, and (c) blast-induced ground motion (BIGM).

$$f_{bx} = c_b\dot{x}_b + k_b x_b,$$
$$f_{by} = c_b\dot{y}_b + k_b y_b, \tag{4}$$

where $c_b = 2\xi_b M_t \omega_b$ is the isolation damping coefficient; $k_b = M_t(2\pi/T_b)^2$ is the isolation stiffness; ω_b is the angular frequency of the isolation system; and $M_t = m_b + \sum_{j=1}^{N} m_j$ is the total mass of the base-isolated building.

The N-Z system, PF system, FPS, and R-FBI are nonlinear isolators, and their force-deformation behaviors are mathematically modeled with and without considering the bidirectional interaction. The restoring forces in the isolation system acting in X and Y directions, respectively, can be obtained as

$$f_{bx} = c_b\dot{x}_b + \alpha k_i x_b + (1-\alpha)F_y h_x, \tag{5a}$$

$$f_{by} = c_b\dot{y}_b + \alpha k_i y_b + (1-\alpha)F_y h_y, \tag{5b}$$

where $k_i = F_y/q$ is the initial stiffness of the isolator and $\alpha = k_b/k_i$ is the postyield to preyield stiffness ratio of the isolator. Furthermore, the nondimensional hysteretic displacement components, h_x and h_y, are evaluated using a set of nonlinear differential equations proposed by Wen [34, 35] and Park et al. [36], respectively, for hysteretic behavior without and with bidirectional interaction. Without accounting for the bidirectional interaction, the values of h_x and h_y can be obtained using the following equations:

$$q\dot{h}_x = A\dot{x}_b + \beta|\dot{x}_b||h_x|^{n-1} - \tau\dot{x}_b|h_x|^n, \tag{6a}$$

$$q\dot{h}_y = A\dot{y}_b + \beta|\dot{y}_b||h_y|^{n-1} - \tau\dot{y}_b|h_y|^n. \tag{6b}$$

On the contrary, considering the bidirectional interaction, h_x and h_y can be evaluated based on the following equation:

$$q\begin{Bmatrix}\dot{h}_x\\ \dot{h}_y\end{Bmatrix} = \begin{bmatrix} A-\beta\mathrm{sgn}(\dot{x}_b)h_x|h_x|^{n-1} - \tau|h_x|^n & -\beta\mathrm{sgn}(\dot{y}_b)h_x|h_y|^{n-1} - \tau h_x h_y \\ -\beta\mathrm{sgn}(\dot{x}_b)h_y|h_x|^{n-1} - \tau h_x h_y & A-\beta\mathrm{sgn}(\dot{y}_b)h_y|h_y|^{n-1} - \tau|h_y|^n \end{bmatrix}\begin{Bmatrix}\dot{x}_b\\ \dot{y}_b\end{Bmatrix}, \tag{7}$$

where $n = 2$ is a parameter used to characterize the smoothness of the nonlinear force-deformation curve of the isolation system, and sgn() represents the signum function. The values of the dimensionless parameters A, β, and τ,

Table 1: Properties of the superstructure and isolation systems of base-isolated buildings.

Component of base-isolated buildings		Parameter	Unit	Values/range of the parameter used in the study
Superstructure		Mass of each floor, m_j	kg	1,427,100
		Base mass, m_b	kg	1,427,100
		Damping ratio, ξ_s	—	0.02–0.08
		Fundamental time period, T^*	s	0.1, 0.2, 0.4, 0.6, and 0.8
		Height of each story, H	m	3.5
Base isolation system	N-Z system	Isolation time period, T_b	s	2.5
		Isolation damping ratio, ξ_b	—	0.05–0.15
		Normalized yield strength, F_0	—	0.025–0.2
		Yield displacement, q	cm	2.5
	LRB	Isolation time period, T_b	s	2, 2.5, 3, and 3.5
		Isolation damping ratio, ξ_b	—	0.025–0.25
	PF system	Friction coefficient, μ_b	—	0.025–0.2
		Yield displacement, q	cm	0.025
	FPS	Isolation time period, T_b	s	2, 2.5, 3, and 3.5
		Friction coefficient, μ_b	—	0.025–0.25
		Yield displacement, q	cm	0.025
	R-FBI	Isolation time period, T_b	s	2.5
		Isolation damping ratio, ξ_b	—	0.05–0.15
		Friction coefficient, μ_b	—	0.025–0.2
		Yield displacement, q	cm	0.025

*The values are given for the fixed-base models of 1, 2, 4, 6, and 8 story buildings, respectively.

respectively, are given as 1, 0.5, and 0.5 for the N-Z system [37]; whereas, the values of A, β, and τ, respectively, are given as 1, 0.1, and 0.9 for the PF system, FPS, and R-FBI [38]. Also, the value of the yield displacement, q, is taken as 2.5 cm for the N-Z system [39], whereas $q = 0.25$ mm is used for sliding isolation systems. Additionally, the damping ratio of the PF system, the postyield stiffness of the PF system, and the damping ratio of the FPS are taken as 0. The yield strength of the N-Z system is evaluated as $F_y = F_0 W_t$, where F_0 and W_t, respectively, are the normalized yield strength of the isolation bearing and the total weight of the base-isolated building. The yield strength of the PF system, FPS, and R-FBI is evaluated as $F_y = \mu_b W_t$, where μ_b is the friction coefficient of the isolation system.

3. Numerical Study

Base-isolated buildings are studied under bidirectional multihazard excitations. The buildings are isolated using five types of base isolation systems, and the behavior of the isolated buildings is assessed under near-fault (NF) earthquakes, far-fault (FF) earthquakes, and blast-induced ground motion (BIGM). The schematic diagram and the idealized model of the base-isolated building studied in this paper are portrayed in Figures 1(a) and 1(b). The masses of all the floors of the building and the base mass are considered to be equal ($m_j = m_b = m$). Also, the lateral stiffnesses of all stories are equal for both X and Y directions. The Rayleigh method is used to construct the damping matrix of the superstructure where the damping ratio of the superstructure (ξ_s) is considered to be 5%. Five building models having different number of stories are studied. The different values of the number of stories of the five buildings are 1, 2, 4, 6, and 8; whereas the fundamental time period (T) values for fixed-base buildings are 0.1 s, 0.2 s, 0.4 s, 0.6 s, and 0.8 s, respectively. Furthermore, the story height (H) of 3.5 m is considered for all the buildings. A summary of the properties of the superstructure and five base isolation systems used in this study is presented in Table 1.

In numerical investigations, the performances of the buildings equipped with five base isolation systems are assessed by studying different response quantities under NF earthquakes, FF earthquakes, and BIGMs. The response quantities, in X and Y directions, that are evaluated and studied include the absolute top floor accelerations ($\ddot{x}_N$ and $\ddot{y}_N$, respectively); top floor displacements (x_N and y_N, respectively), relative to the ground; isolator displacements (x_b and y_b, respectively), relative to the ground; normalized base shears (V_x^n and V_y^n, respectively); total superstructure drift ratio (Δ_{total}^x and Δ_{total}^y, respectively); and maximum interstory drift ratio ($\text{Max}(\Delta_j^x)$ and $\text{Max}(\Delta_j^y)$, respectively). The total superstructure drift ratio is obtained as the ratio of the total drift of the superstructure to the total height of the superstructure. Furthermore, the maximum interstory drift ratio is obtained as the maximum of the peak values of the interstory drift ratios of all the stories of the building. In addition, resultant top floor acceleration ($\ddot{\sigma}_N$), resultant top floor displacement (σ_N), resultant isolator displacement (σ_b), resultant normalized base shear (V_σ^n), resultant total superstructure drift ratio ($\Delta_{\text{total}}^\sigma$), and resultant maximum interstory drift ratio ($\text{Max}(\Delta_j^\sigma)$) are also studied.

3.1. Bidirectional Multihazard Condition Considered in the Study. The current study focuses on the investigation of the multihazard behavior of base-isolated buildings under bidirectional base excitations of different types. The near-fault (NF) earthquake ground motions, far-fault (FF) earthquake ground motions, and blast-induced ground motions (BIGMs) are imparted on buildings isolated using various

Table 2: Details of the six bidirectional earthquake ground motions used in the study.

Sl. no.	Earthquake event	Date of event	R_{rup} (km)	Record (NF/FF)	Notation	Component	Direction	PGA (g)
1	Imperial Valley	Oct 15, 1979	3.95	Array #5 (NF)	IV1979	Normal (N)	X	0.37
						Parallel (P)	Y	0.55
2	Loma Prieta	Oct 18, 1989	3.88	LGPC (NF)	LP1989	Normal (N)	X	0.57
						Parallel (P)	Y	0.61
3	Northridge	Jan 17, 1994	5.30	Sylmar (NF)	NR1994	Normal (N)	X	0.73
						Parallel (P)	Y	0.59
4	Imperial Valley	Oct 15, 1979	22.03	Delta (FF)	IV1979F	Normal (N)	X	0.24
						Parallel (P)	Y	0.35
5	Loma Prieta	Oct 18, 1989	24.82	HDA (FF)	LP1989F	Normal (N)	X	0.27
						Parallel (P)	Y	0.28
6	Northridge	Jan 17, 1994	23.41	Century City (FF)	NR1994F	Normal (N)	X	0.26
						Parallel (P)	Y	0.22

base isolation systems. Six recorded bidirectional earthquake ground motion records are used in this investigation. Three of the six earthquake ground motion records (a) the 1979 Imperial Valley with the closest distance to rupture plane, R_{rup}, of 3.95 km (IV1979); (b) the 1989 Loma Prieta, R_{rup} = 3.88 km (LP1989); and (c) the 1994 Northridge, R_{rup} = 5.3 km (NR1994) are near-fault earthquake ground motions. The remaining three earthquake ground motion records (a) the 1979 Imperial Valley, R_{rup} = 22.03 km (IV1979F); (b) the 1989 Loma Prieta, R_{rup} = 24.82 km (LP1989F); and (c) the 1994 Northridge, R_{rup} = 23.41 km (NR1994F) are far-fault earthquake ground motions. Table 2 provides the date of the event, the recording station, the closest distance to rupture plane, the peak ground acceleration (PGA) in gravitation acceleration (g) unit, and other relevant details of the earthquake ground motion data. In the table, the two components of each of the six earthquake events are presented, which are applied as base excitations in the X direction ($\ddot{x}_g$) and Y direction ($\ddot{y}_g$) simultaneously.

The extent of ground vibration due to blast is influenced by various parameters, such as the type of the explosive, the weight of the explosive, the type of the ground medium, and the distance to the charge. In this study, the blast-induced ground motion is represented mathematically using the function proposed by Carvalho and Battista [40]. The exponentially decaying BIGM acceleration, $\ddot{U}_g(t)$, that is imparted on the base-isolated buildings with an angle of attack (θ) measured from the X-axis (Figure 1(c)) can be evaluated as

$$\ddot{U}_g(t) = -\left(\frac{1}{t_d}\right)\overline{\ddot{u}}_g\, e^{-\left(t/t_d\right)}, \tag{8}$$

where t is the time instant; $t_d = R/C_p$ is the arrival time; R is the distance to the charge; $\overline{\ddot{u}}_g = 0.3607\,(Q/V)^{0.2872}\,(R/Q^{(1/3)})^{-1.3375}$ is the peak particle velocity (PPV) [41]; $C_p = \sqrt{E/\rho}$ is the velocity of wave propagation through the soil medium; E and ρ, respectively, are Young's modulus and the average density of the soil medium; V is the charge chamber volume in m^3; and Q is the weight of the equivalent trinitrotoluene (TNT) charge in kg.

The values of C_p, R, and V used in this study are 5280 m/s, 50 m, and 1000 m^3, respectively, whereas the TNT charge weight (Q) values of 50 t, 75 t, and 100 t are considered to evaluate BIGM acceleration. Additionally, the obtained BIGM acceleration is applied to the base-isolated buildings with angle of attack (θ) values of 0°, 15°, 30°, and 45°. For BIGM acceleration acting with an angle of attack θ from the X-axis, the X component of BIGM can be obtained as $\ddot{x}_g = \ddot{U}_g \cos(\theta)$, whereas the Y component can be computed as $\ddot{y}_g = \ddot{U}_g \sin(\theta)$. The time histories of the near-fault earthquakes, far-fault earthquakes, and BIGMs used in the study are presented in Figure 2, whereas the Fourier spectra of the three types of excitations are given in Figure 3.

3.2. Effect of Bidirectional Interaction. The two components of the considered earthquake ground motions and BIGMs are applied to the building as base excitations acting in X and Y directions simultaneously. The resultant response quantity can then be evaluated as $\psi_r = \sqrt{\psi_X^2 + \psi_Y^2}$, where ψ_r is the resultant value of any response quantity, ψ_X is the value of the response quantity in the X direction, and ψ_Y is the value of the response quantity in the Y direction.

For the linear base isolation system, laminated rubber bearing (LRB), the response of the building under bidirectional excitations can be obtained by evaluating the response of the building under the two components of the excitations applied in X and Y directions without special consideration of the bidirectional interaction at the isolation level. However, this approach may lead to incorrect results for the buildings isolated by nonlinear base isolation systems. When buildings isolated by nonlinear base isolators are subjected to bidirectional excitations, the force that is acting on the base isolators is derived from the excitations acting in both X and Y directions. Therefore, when the resultant force in the isolator equals the yield force, the postyield behavior of the isolation system is activated.

The X and Y components of the yield strength of the isolator are influenced by relative magnitudes of the isolator forces in X and Y directions. The relationship between the normalized yield strength (F_0), the normalized yield strength in the X direction (F_0^X), and the normalized yield strength in the Y direction (F_0^Y) is given as $(F_0)^2 = (F_0^X)^2 + (F_0^Y)^2$. The graphical representation of relationship between F_0^X, F_0^Y, and F_0 is depicted in Figure 4, as a function of the angle (direction) of the resultant isolator force measured from the X-axis (φ).

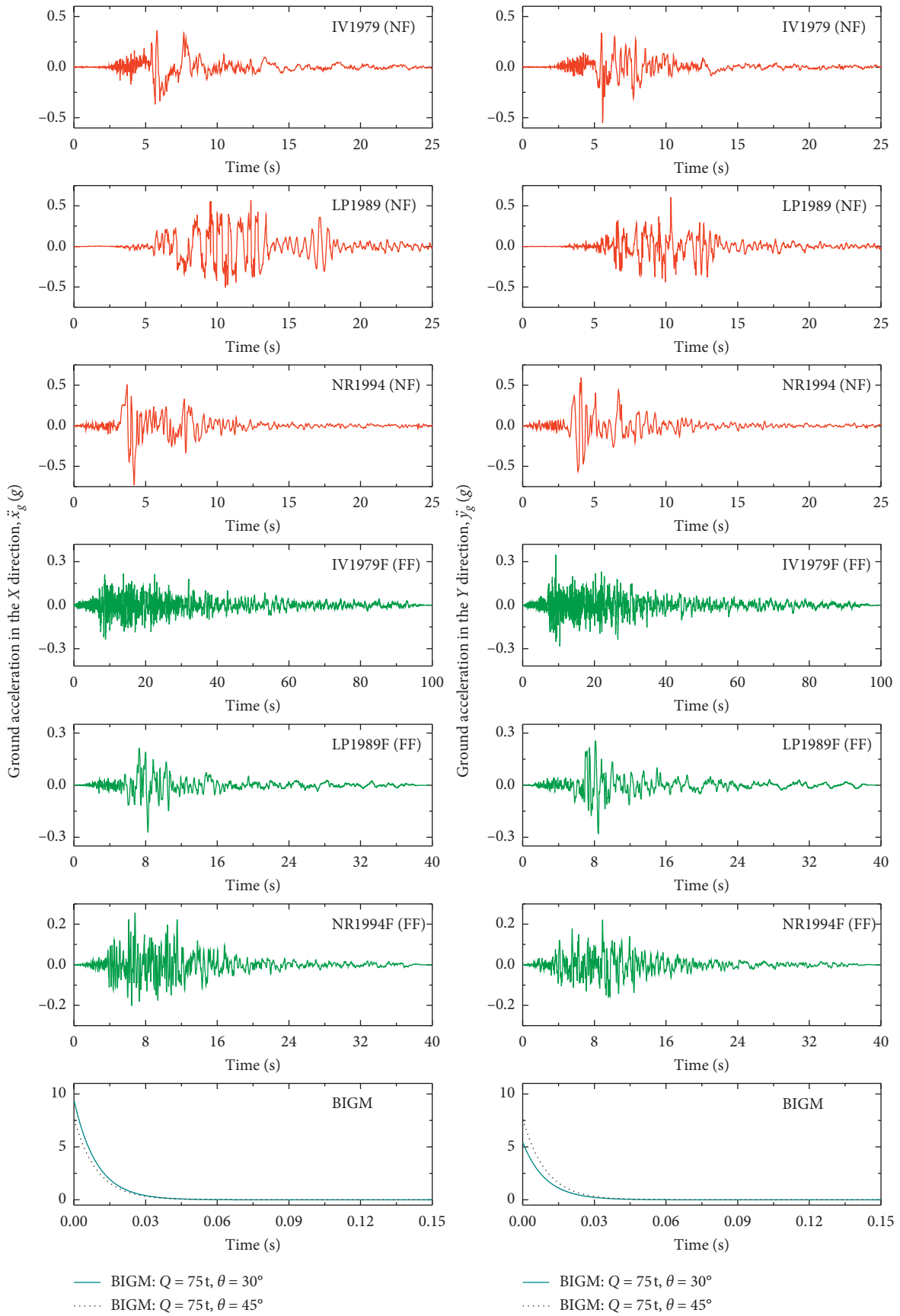

Figure 2: Time histories of NF earthquakes, FF earthquakes, and BIGMs used in the study.

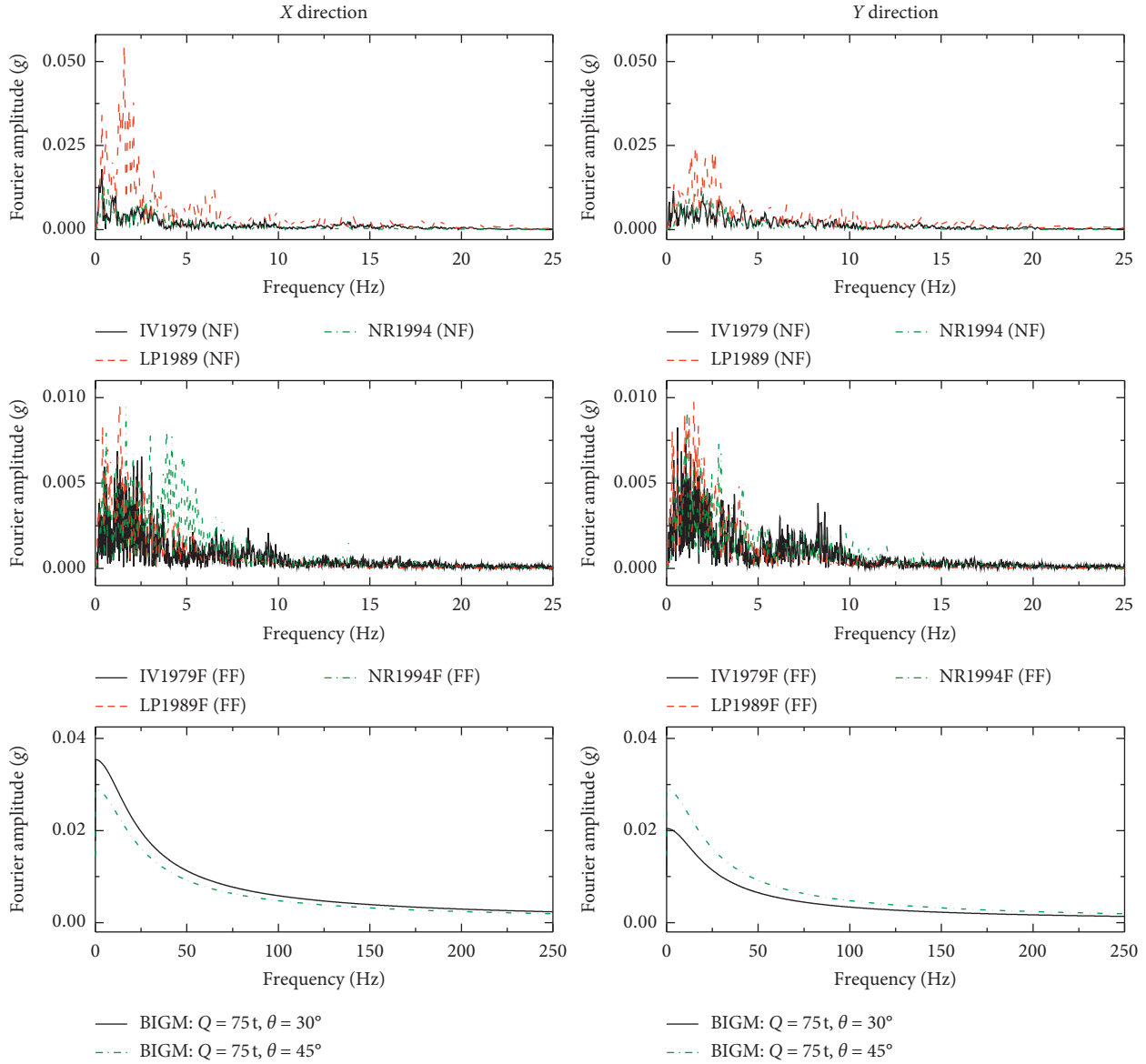

Figure 3: Fourier spectra of NF earthquakes, FF earthquakes, and BIGMs used in the study.

If the response of the building is evaluated independently for excitations acting in X and Y directions, it results in neglecting the effect of the bidirectional interaction. For example, the response of a four-story building with a fixed-base fundamental time period (T) of 0.4 s and a superstructure damping ratio (ξ_s) of 0.05 isolated by the FPS is presented in Figures 5 and 6. In Figure 5, the time histories of the top floor acceleration of the four-story building isolated by the FPS ($T_b = 2.5$ s and $\mu_b = 0.1$) with and without the consideration of bidirectional interaction are presented. Furthermore, the force-deformation plots of the FPS, with and without the consideration of bidirectional interaction under (a) LP1989, (b) LP1989F, and (c) BIGM, $Q = 75$ t and $\theta = 30^\circ$, are shown in Figure 6. The time history plots and the force-deformation behavior depicted in Figures 5 and 6 show that the response obtained with and without the consideration of the bidirectional interaction are significantly different.

Therefore, a detailed comparative study is conducted for determining the degree to which the values of the different response quantities of base-isolated buildings are influenced due to the bidirectional interaction. The response quantities of the buildings isolated by the N-Z system, PF system, FPS, and R-FBI are studied under various bidirectional base excitations with and without the consideration of the bidirectional interaction. The percentage variation between the response quantities of the building with and without the consideration of the bidirectional interaction is evaluated as

$$\Delta\psi = \frac{(\psi_{\text{Int}} - \psi_{\text{NoInt}})}{\psi_{\text{NoInt}}} \times 100, \tag{9}$$

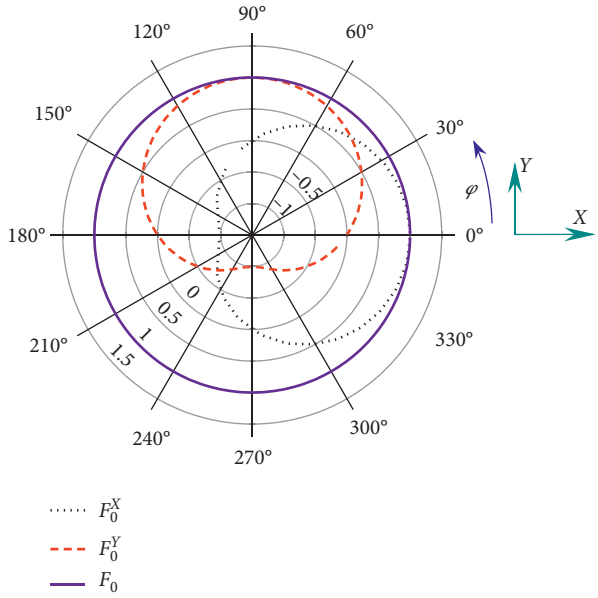

FIGURE 4: The relationship between the normalized yield strength of the isolator (F_0) and its components in X and Y directions (F_0^X and F_0^Y, respectively) for different directions (angle, φ, measured from the X-axis) of the resultant isolator force.

where $\Delta\psi$ is the percentage difference in a response quantity; ψ_{NoInt} is the peak value of the resultant response quantity when the bidirectional interaction is not considered; and ψ_{Int} is the peak value of the resultant response quantity when the bidirectional interaction is considered.

The values of $\Delta\psi$ corresponding to the resultant top floor acceleration, resultant isolator displacement, and resultant base shear of the four-story building equipped with four nonlinear isolators under NF earthquakes, FF earthquakes, and BIGMs are presented in Figure 7. It is shown in the figure that, for all cases, the resultant top floor acceleration and the resultant base shear are overestimated if the bidirectional interaction is neglected. On the contrary, the neglection of the bidirectional interaction is observed to result in the underestimation of the resultant isolator displacement response. The underestimation and overestimation of the response quantities arise because of the modeling approach that neglects the bidirectional interaction. When the bidirectional interaction is neglected, the isolation system is modeled in a way such that the postyield behavior is exhibited at a larger value of the normalized resultant isolator force than that of the case where the bidirectional interaction is considered. This results in the modeling of the isolation system with increased initial stiffness and reduced flexibility under bidirectional excitations. Consequently, a smaller value of resultant isolator displacement and larger values of resultant top floor acceleration and resultant base shear are obtained for the case where the bidirectional interaction is not considered.

The extent of the overestimation and underestimation of the response quantities varies depending on the excitation and the isolation system. For NF earthquake ground motions, the neglection of the bidirectional interaction results in the overestimation of the resultant top floor acceleration and the resultant base shear by up to 44.5% and 31.9%, respectively. On the contrary, the resultant isolator displacement is underestimated by up to 32%. For FF earthquakes, the neglection of the bidirectional interaction resulted in the overestimation of the resultant top floor acceleration and the resultant base shear by up to 31.6% and 33.5%, respectively. Also, the resultant isolator displacement is underestimated by up to 81.2%. The resultant top floor acceleration and the resultant base shear are overestimated by up to 29.3% due to the neglection of the bidirectional interaction for the base-isolated buildings exposed to BIGMs. Furthermore, the resultant isolator displacement is underestimated by up to 27.6%. Consequently, it can be concluded that, when the bidirectional interaction is neglected, the resultant top floor acceleration and resultant base shear are overestimated, and the resultant isolator displacement is underestimated considerably under all three types of excitations. This influences the multihazard response of the base-isolated buildings significantly. Therefore, the bidirectional interaction should be considered to capture the behavior of base-isolated buildings under bidirectional NF earthquakes, FF earthquakes, and BIGMs with adequate accuracy.

3.3. Multihazard Response of Base-Isolated Buildings under Bidirectional Excitations. Four-story base-isolated buildings are studied under NF earthquakes, FF earthquakes, and BIGMs to understand the effect of the various base isolation systems on the behavior of the buildings under multihazard loading. The base-isolated buildings are subjected to bidirectional excitations, and their response quantities in X and

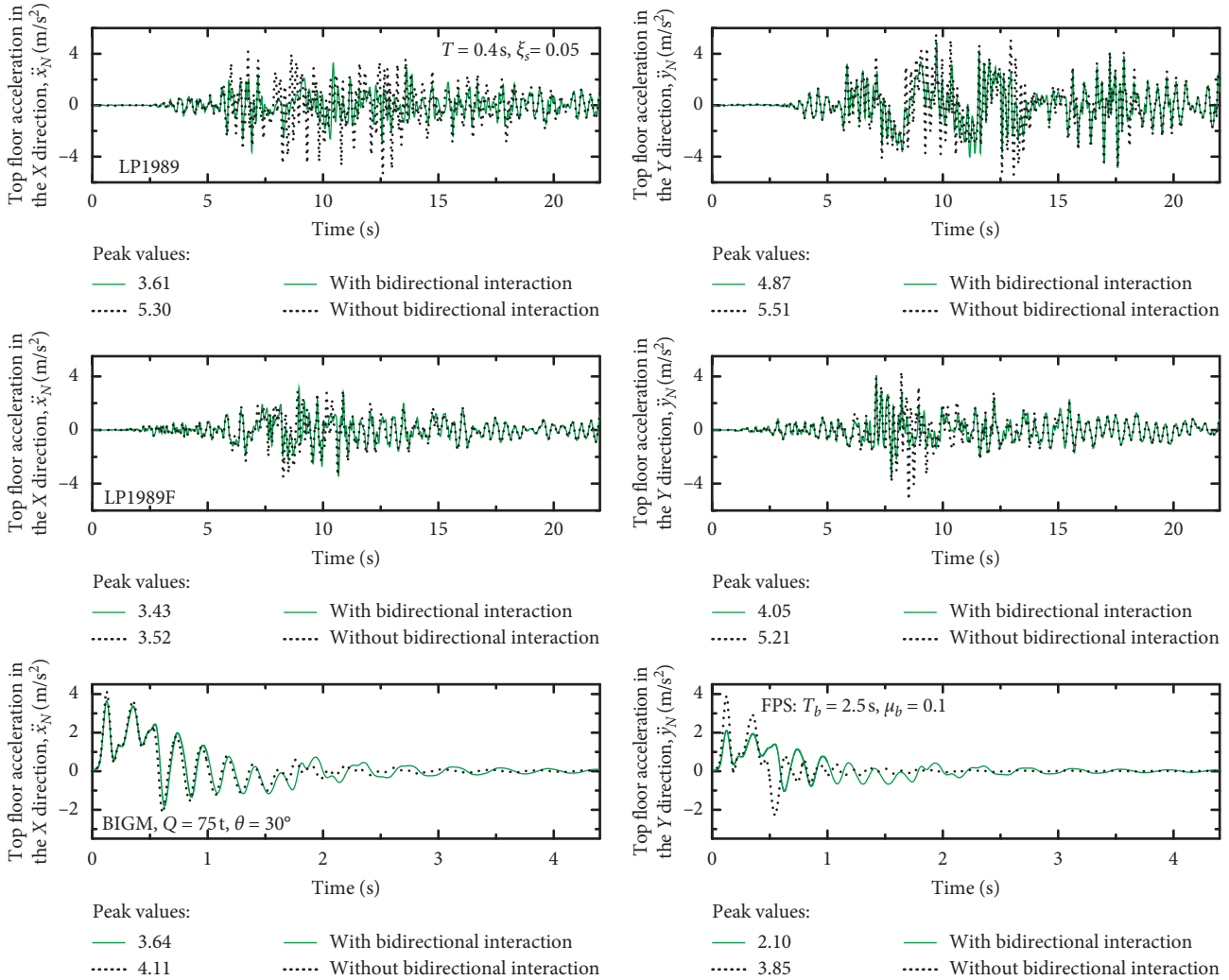

FIGURE 5: Top floor acceleration response history of a four-story base-isolated building with and without the consideration of bidirectional interaction.

Y directions and the resultant response quantities are investigated considering the bidirectional interaction.

3.3.1. Response of the Building Isolated by the N-Z System. The trends of the peak values of the X component, Y component, and resultant response quantities (top floor acceleration and isolator displacement) of a four-story building equipped with the N-Z system are presented in Figure 8. The fixed-base fundamental time period (T) of the four-story building used in this investigation is 0.4 s, whereas a superstructure damping ratio (ξ_s) of 0.05 is considered. The isolation time period (T_b) of 2.5 s, yield displacement (q) of 2.5 cm, and isolation damping ratio (ξ_b) of 0.075 are used. Moreover, the normalized yield strength (F_0) of the N-Z system varied from 0.025 to 0.2.

The results presented in Figure 8 depict the influence of the normalized yield strength (F_0) of the N-Z system on the response quantities of the base-isolated building under NF earthquakes, FF earthquakes, and BIGMs. For NF earthquakes and FF earthquakes, the average trends of the absolute top floor acceleration and the isolator displacement are also presented in the figure. The values of the response quantities for the fixed-base building are also presented for comparison. For all three types of excitations, the absolute top floor acceleration response of the building in X, Y, and resultant directions show a considerable reduction as compared to the fixed-base response (FBR). This reduction highlights the benefit of base isolation in suppressing the undesirable effect of NF earthquakes, FF earthquakes, and BIGMs.

The bidirectional response of the base-isolated building under BIGMs with different values of equivalent TNT charge weight (Q) and the angle of attack (θ) is also presented. The influence of Q on the response quantities is observed from the results obtained for BIGMs with a 30° angle of attack and equivalent TNT charge weight (Q) values of 50 t, 75 t, and 100 t. As expected, the response quantities are observed to be more for the higher value of TNT charge weight. In addition, the influence of the angle of attack is studied by taking BIGMs with 75 t equivalent

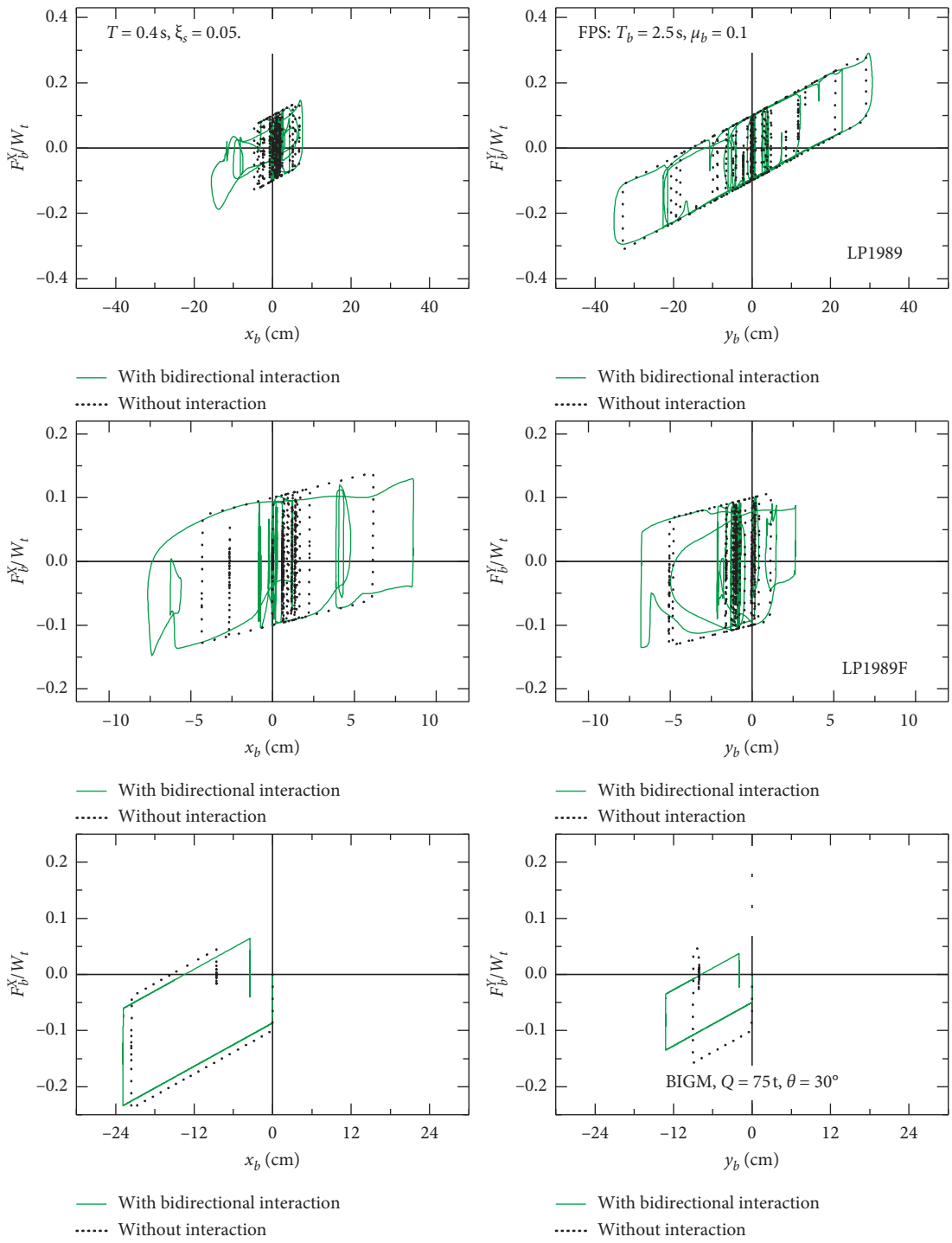

Figure 6: Force-deformation curve of the FPS system with and without the consideration of bidirectional interaction.

TNT charge weight and angle of attack (θ) values of 0°, 15°, 30°, and 45°. As the angle of attack increases, the response in the Y direction is observed to be increasing and the same in the X direction is observed to be decreasing. This is primarily because the building is symmetrical about X and Y axes, and the component of BIGM along the Y direction increases with an increasing angle of attack. The results presented in Figure 8 show that the top floor acceleration and isolator displacement response quantities show a similar trend for different values of equivalent the TNT charge weight and angle of attack. Also, for the four-story building with similar properties in the X and Y directions, the resultant value of the response quantities under BIGMs having different values of the angle of attack are found to be the same. In addition, an increase in the normalized yield strength results in a decreasing trend of the resultant isolator displacement for the base-isolated buildings under all three types of

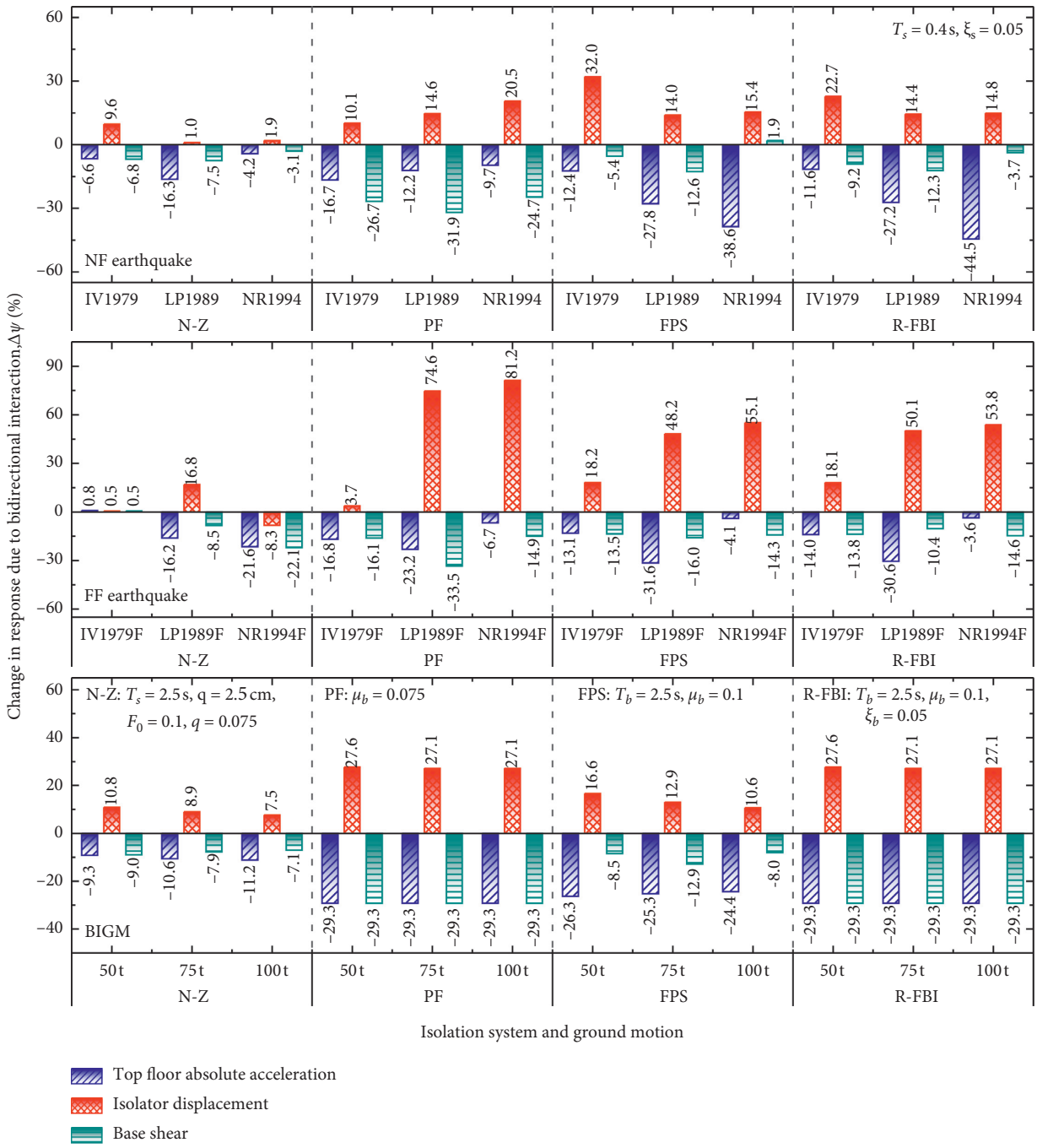

Figure 7: The effect of bidirectional interaction on the top floor acceleration, isolator displacement, and base shear response under earthquake and blast-induced ground motions.

excitations. On the contrary, the resultant top floor acceleration increases with the normalized yield strength for the base-isolated buildings under FF earthquake and BIGM. Furthermore, NF earthquakes result in an initial reduction of the resultant top floor acceleration, up to a certain value of the normalized yield strength of the isolator, and further increment of the normalized yield strength results in an increasing trend of the top floor acceleration.

To investigate the behavior of the base-isolated buildings further, under the multihazard scenario of earthquake and BIGM, the top floor acceleration, top floor displacement, isolator displacement, normalized base shear, total superstructure drift ratio, and maximum interstory drift ratio are evaluated under bidirectional NF earthquakes, FF earthquakes, and BIGMs. The X, Y, and resultant components of the response quantities are assessed for the buildings equipped with the N-Z system, LRB, PF system, FPS, and

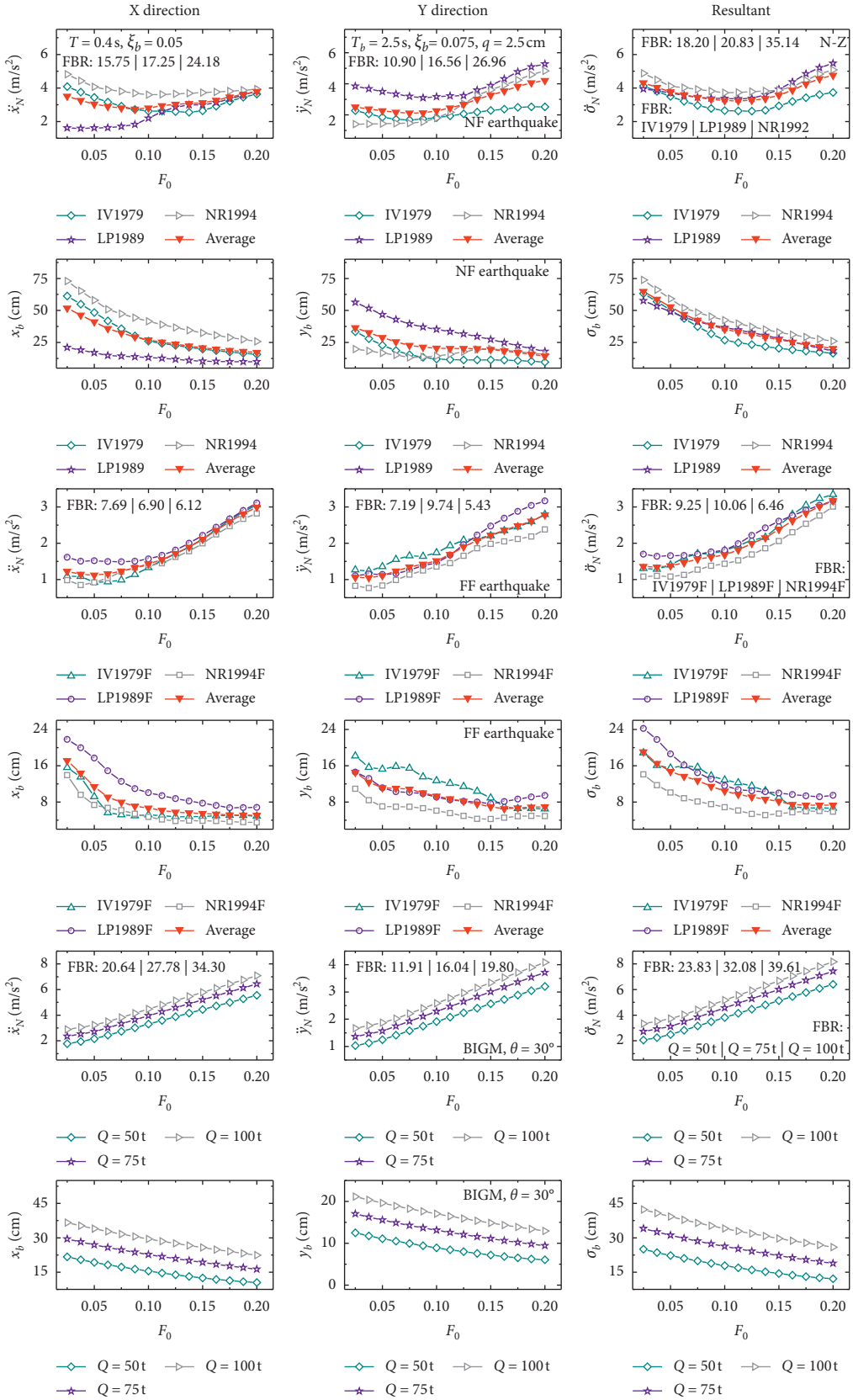

Figure 8: Continued.

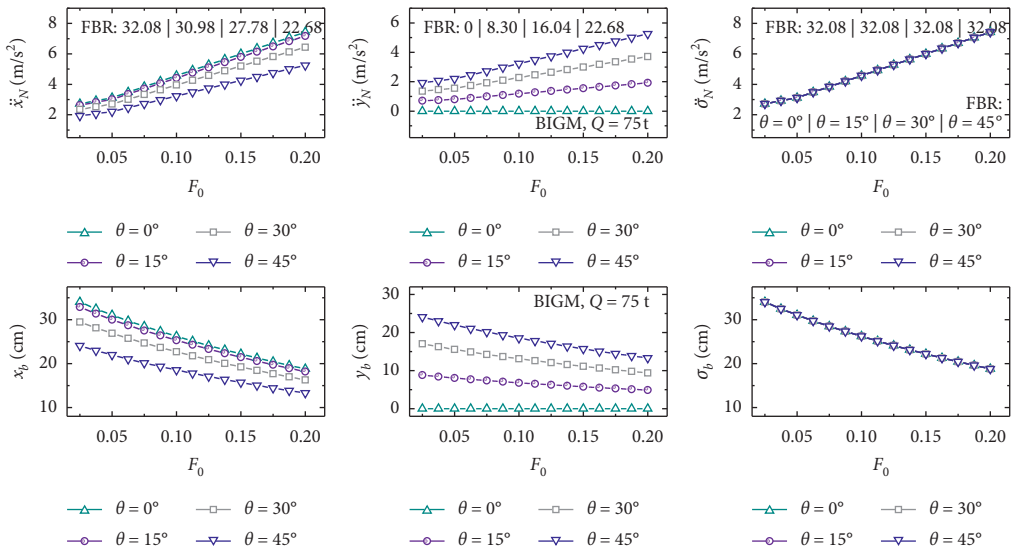

Figure 8: The response of a four-story building isolated by the N-Z system under NF earthquakes, FF earthquakes, and BIGMs.

R-FBI under multiple hazards. The average values of the response quantities obtained under IV1979, LP1989, and NR1994 earthquake ground motions are taken to obtain representative trends for the NF earthquake case. Similarly, the average values of the response quantities obtained under IV1979F, LP1989F, and NR1994F earthquake ground motions are taken to obtain representative trends for the FF earthquake case. The average response trends are obtained for the buildings isolated by the five base isolation systems under NF and FF earthquakes, which are then compared with the response trends obtained for the base-isolated buildings subjected to BIGM.

The comparison of the performance of the N-Z system ($T_b = 2.5$ s and $q = 2.5$ cm) under NF earthquake, FF earthquake, and BIGM is depicted in Figure 9 for the four-story building ($T = 0.4$ s and $\xi_s = 0.05$). The effect of the normalized yield strength (F_0) of the N-Z system on the resultant top floor acceleration ($\ddot{\sigma}_N$), resultant top floor displacement (σ_N), resultant isolator displacement (σ_b), resultant normalized base shear (V_σ^n), resultant total superstructure drift ratio ($\Delta_{\text{total}}^\sigma$), and resultant maximum interstory drift ratio ($\text{Max}(\Delta_j^\sigma)$) is presented. The trends of the six response quantities obtained for the N-Z system with different isolation damping ratio (ξ_b) values are similar. For all three types of excitations, the resultant top floor displacement and resultant isolator displacement are observed to show reduction as the value of the normalized yield strength of the N-Z system (F_0) increases. On the contrary, the influence of the normalized yield strength on the resultant top floor acceleration, resultant normalized base shear, resultant total superstructure drift ratio, and resultant maximum interstory drift ratio is found to be different under NF earthquakes, FF earthquakes, and BIGMs. For the base-isolated building under NF earthquakes, an increase in the normalized yield strength of the N-Z system results in an initial reduction of the four response quantities. However, an increase in F_0 beyond the value of about 0.13 results in an upsurge of the values of the resultant top floor acceleration, resultant normalized base shear, resultant total superstructure drift ratio, and resultant maximum interstory drift ratio. For the base-isolated building subjected to FF earthquake ground motions, an increase in the F_0 typically results in an increment of $\ddot{\sigma}_N$, V_σ^n, $\Delta_{\text{total}}^\sigma$, and $\text{Max}(\Delta_j^\sigma)$, except for a relatively flat trend for small values of F_0 (up to 0.065) with isolation damping ratio, ξ_b, of 0.05 and 0.075. Furthermore, BIGM results in consistent increasing trends of $\ddot{\sigma}_N$, V_σ^n, $\Delta_{\text{total}}^\sigma$, and $\text{Max}(\Delta_j^\sigma)$ for an increase in F_0.

3.3.2. Response of the Building Isolated by LRB. The behavior of the building isolated by LRB under the three types of excitations is assessed considering different values of the isolation time period (T_b) and isolation damping ratio (ξ_b). The isolation damping ratio varied from 0.025 to 0.25, whereas four different values of the isolation time period (2 s, 2.5 s, 3 s, and 3.5 s) are considered. The influence of the isolation damping ratio on the response quantities of the four-story base-isolated building for the three types of excitations is depicted in Figure 10. The trends of the resultant top floor acceleration, resultant top floor displacement, resultant isolator displacement, resultant normalized base shear, resultant total superstructure drift ratio, and resultant maximum interstory drift ratio observed under earthquake excitation, for an increase in the isolation damping ratio, are similar. The values of the six response quantities reduce with an increase in the isolation damping ratio both under NF and FF earthquakes. For the building subjected to BIGM, the resultant normalized base shear, resultant total superstructure drift ratio, and resultant maximum interstory drift ratio show a relatively flat trend with an increase in the isolation damping ratio. On the contrary, an increase in the isolation damping ratio results in the reduction of the

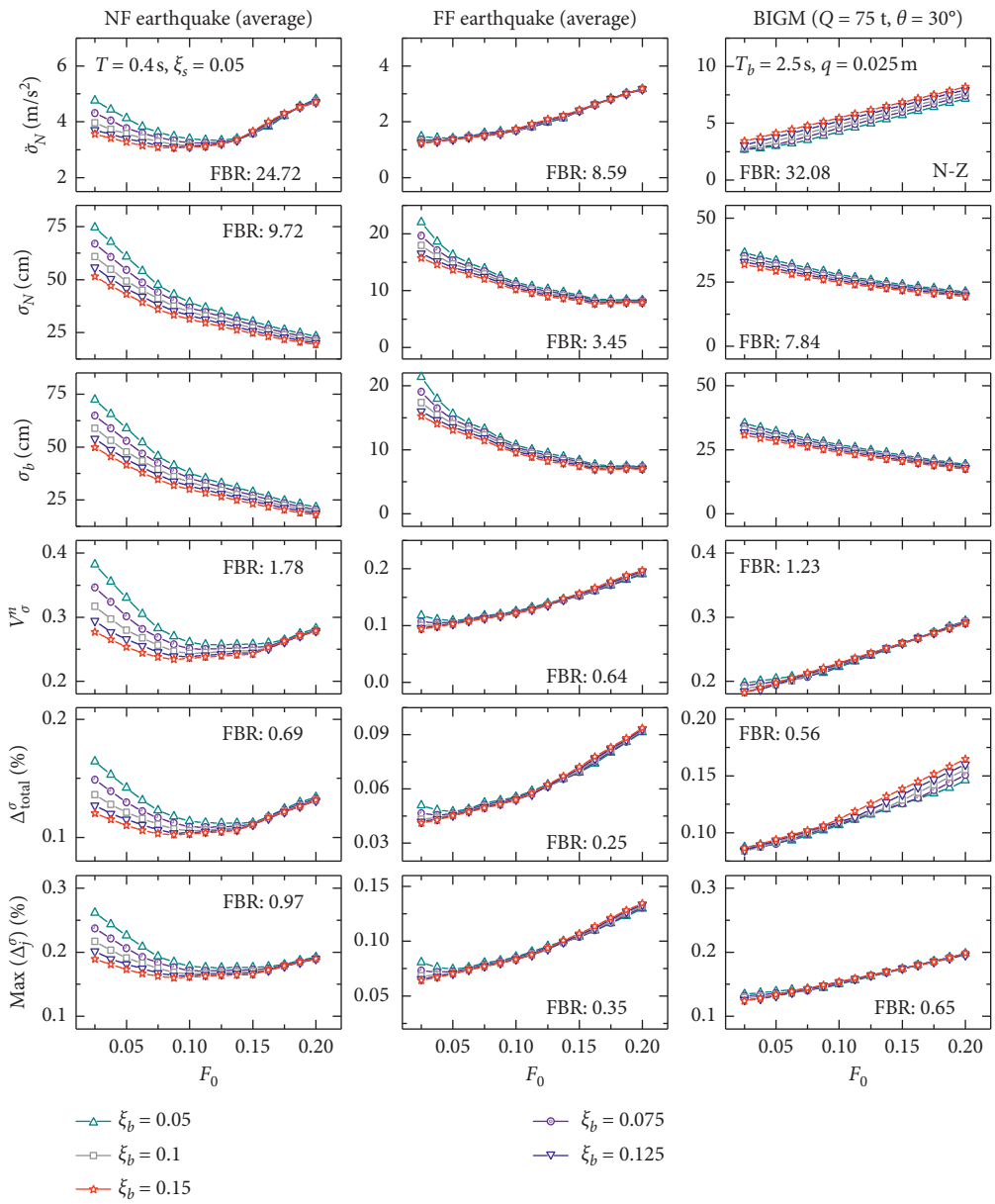

Figure 9: The effect of the normalized yield strength (F_0) and the isolation damping ratio (ξ_b) on the response of a four-story building isolated by the N-Z system under earthquake and BIGM.

resultant top floor displacement and resultant isolator displacement, whereas the resultant top floor acceleration increases with an increase in the isolation damping ratio.

3.3.3. Response of the Building Isolated by the PF System. The performance of the PF system under NF earthquake, FF earthquake, and BIGM is evaluated by varying the friction coefficient of the isolation system (μ_b) from 0.025 to 0.25. The influence of the friction coefficient of the isolation system on the response quantities of the four-story base-isolated building under the three types of excitations is presented in Figure 11. The results plotted in the figure show that the trends of the six response quantities are similar for NF earthquakes, FF earthquakes, and BIGMs. For all the three types of excitations, the top floor displacement and isolator displacement show a decreasing trend for an increase in the friction coefficient. Moreover, as the friction coefficient of the PF system increases, the top floor acceleration, base shear, total superstructure drift ratio, and maximum interstory drift ratio increase. Also, the comparison of the residual resultant isolator displacements of the building equipped with the PF system to that of the other isolation systems is presented in Table 3. Because the pure friction system lacks restoring capacity, the building isolated by the PF

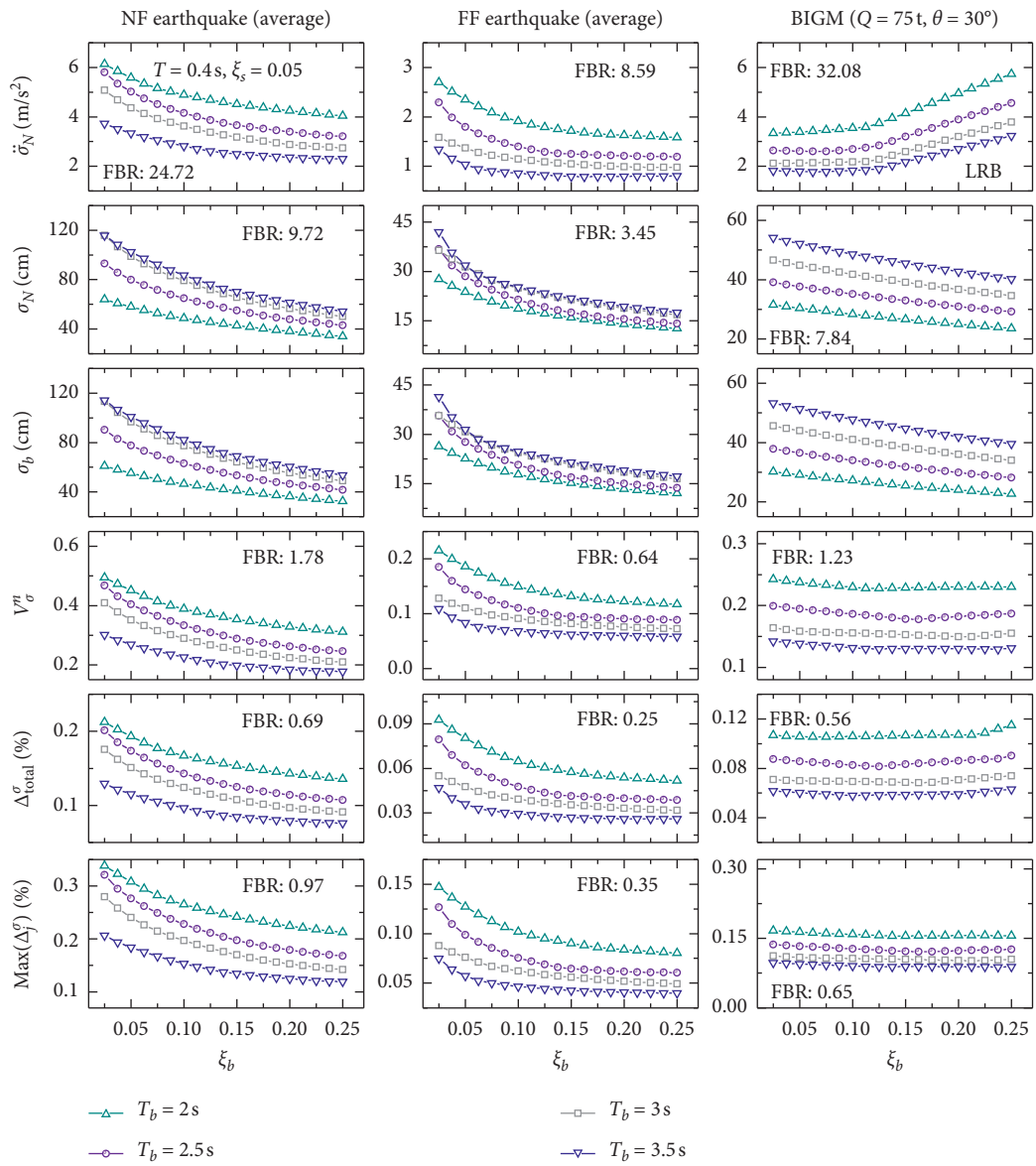

FIGURE 10: The effect of the isolation damping ratio (ξ_b) and the isolation time period (T_b) on the response of a four-story building isolated by LRB under earthquake and BIGM.

system is observed to be prone to large residual displacements under the three types of excitations.

3.3.4. Response of the Building Isolated by the FPS. The behavior of the four-story building isolated by the FPS under the independent multihazard scenario of earthquake and BIGM is presented in Figure 12. The isolation time period (T_b) values of 2 s, 2.5 s, 3 s, and 3.5 s are considered for the FPS, whereas the coefficient of friction of the isolation system (μ_b) is varied from 0.025 to 0.25. For small values of the friction coefficient of the FPS (i.e., approximately up to $\mu_b = 0.075$), the resultant top floor acceleration shows small reduction for an increase in μ_b under NF earthquakes, whereas the resultant top floor acceleration exhibits an increasing trend for an increase in the friction coefficient of the FPS beyond 0.075. Under FF earthquake and BIGM, the resultant top floor acceleration shows a steady increase with an increase in μ_b. An increase in the friction coefficient of the FPS affects the resultant top floor displacement and resultant isolator displacement similarly. Both the response quantities reduce with an increase in the friction coefficient under NF earthquake, FF earthquake, and BIGM. Under NF earthquake, the resultant normalized base shear, resultant total superstructure drift ratio, and resultant maximum interstory drift ratio initially reduce with an increase in the friction coefficient of the isolator, and after a certain value of μ_b, the three response quantities start to show an increasing trend. For FF earthquake, the three response quantities show a small reduction for small values of the friction coefficient of the FPS ($\mu_b \leq 0.05$). For

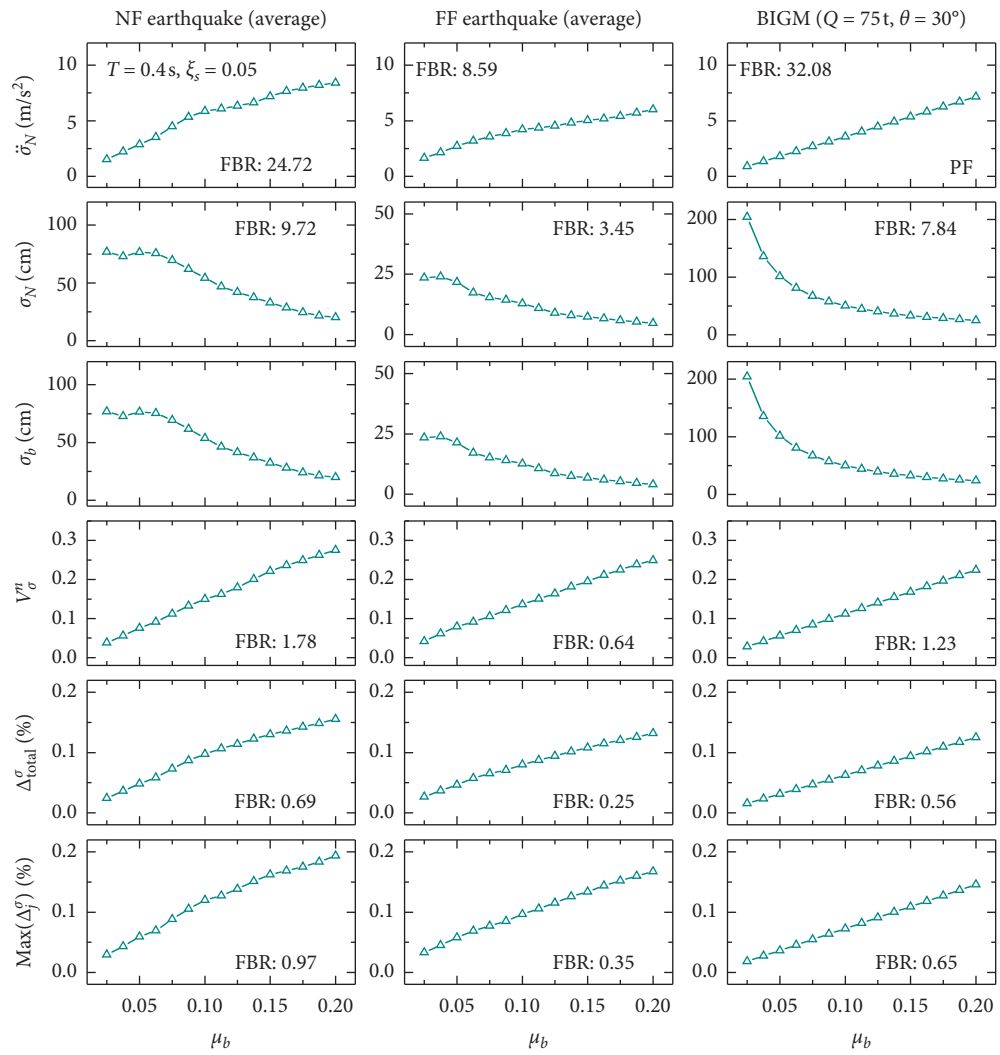

FIGURE 11: The response of a four-story building $T = 0.4$ s; $\xi_s = 0.05$ isolated by the PF system under NF earthquake, FF earthquake, and BIGM.

friction coefficient values beyond 0.05, the trends are reversed, and the three response quantities increase with an increase in μ_b. Moreover, an increase in μ_b results in a consistent increment of the resultant normalized base shear, resultant total superstructure drift ratio, and resultant maximum interstory drift ratio of the base-isolated building under BIGM.

3.3.5. Response of the Building Isolated by the R-FBI. The performance of the four-story building equipped with the R-FBI under NF earthquake, FF earthquake, and BIGM is portrayed in Figure 13. The isolation time period (T_b) of the R-FBI is taken as 2.5 s; the isolation damping ratio (ξ_b) values of 0.05, 0.075, 0.1, 0.125, and 0.15 are considered; and the coefficient of friction of the isolation system (μ_b) is varied from 0.025 to 0.2. The overall behavior of the building isolated by the R-FBI is similar to that of the building equipped with the FPS, except for a small difference in the trends of the resultant normalized base shear, resultant total superstructure drift ratio, and resultant maximum interstory drift ratio under FF earthquakes. For the building equipped with the R-FBI subjected to FF earthquakes, an increase in the friction coefficient of the isolation system results in a consistent increment of the resultant normalized base shear, resultant total superstructure drift ratio, and resultant maximum interstory drift ratio.

For the building subjected to NF earthquakes, the top floor displacement, isolator displacement, normalized base shear, total superstructure drift ratio, and maximum interstory drift ratio are influenced significantly by the damping ratio of the R-FBI. For small values of the friction coefficient of the isolator, a larger isolation damping ratio results in smaller values of the five response quantities. However, as the friction coefficient of the R-FBI increases, the influence of the damping ratio of the isolation system diminishes. Moreover, the effect of the damping ratio of the R-FBI on the top floor acceleration is less under NF earthquakes, irrespective of the value of the friction coefficient. Under FF earthquakes, the top floor acceleration, normalized base shear, total

Table 3: Residual resultant isolator displacements of four-story base-isolated buildings under NF earthquakes, FF earthquakes, and BIGMs.

Excitation		Residual resultant isolator displacement for buildings ($T_s = 0.4$ s, $\xi_s = 0.05$) equipped with different isolation systems (cm)				
		LRB ($T_b = 2$ s and $\xi_b = 0.1$)	N-Z ($T_b = 2$ s, $F_0 = 0.05$, and $\xi_b = 0.1$)	PF ($\mu_b = 0.05$)	FPS ($T_b = 2$ s and $\mu_b = 0.05$)	R-FBI ($T_b = 2$ s, $\mu_b = 0.05$, and $\xi_b = 0.1$)
NF earthquake	IV1979	1.24	0.61	102.50	0.41	0.56
	LP1989	1.21	0.91	41.74	0.24	0.23
	NR1994	0.48	0.19	16.98	0.38	0.13
FF earthquake	IV1979F	0.62	0.12	11.63	0.62	0.60
	LP1989F	2.82	0.59	33.89	0.07	0.10
	NR1994F	0.66	0.51	5.19	0.55	0.53
BIGM	$Q = 75$ t; $\theta = 30^\circ$	0.06	0.02	101.32	2.26	1.88
	$Q = 75$ t; $\theta = 45^\circ$	0.06	0.02	101.32	2.26	1.88

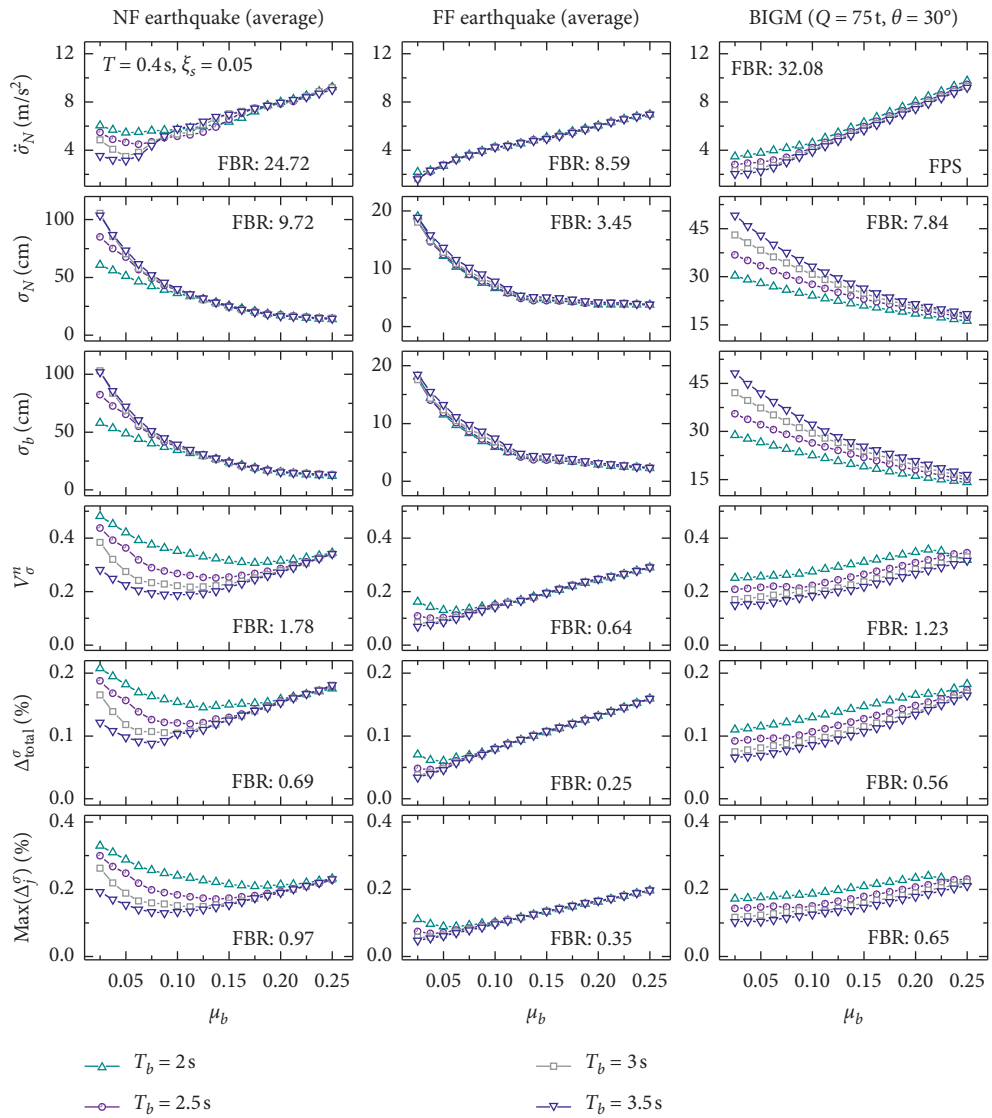

Figure 12: The effect of the friction coefficient of the isolator (μ_b) and the isolation time period (T_b) on the response of a four-story building isolated by the FPS under earthquake and BIGM.

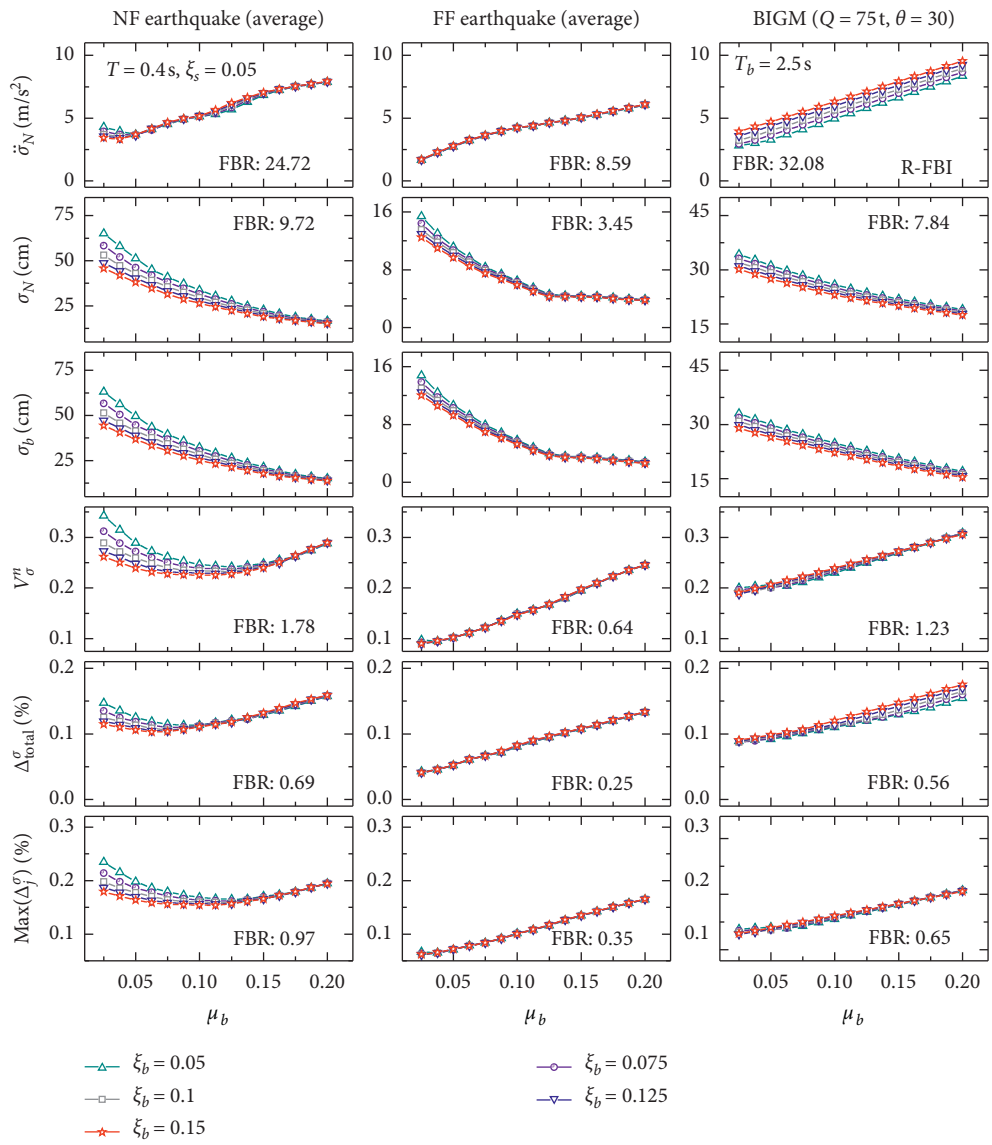

FIGURE 13: The effect of the friction coefficient of the isolator (μ_b) and the isolation damping ratio (ξ_b) on the response of a four-story building isolated by the R-FBI system under earthquake and BIGM.

superstructure drift ratio, and maximum interstory drift ratio are not influenced significantly by the damping ratio of the R-FBI. Similarly, the influence of the isolation damping on the normalized base shear and the maximum interstory drift ratio is small for the base-isolated building under BIGM. For the base-isolated building with small values of the friction coefficient of the R-FBI that is subjected to FF earthquakes and BIGMs, the top floor displacement and isolator displacement reduce as the damping ratio of the isolation system increase. On the contrary, the top floor acceleration and total superstructure drift ratio increase as the damping ratio increases for the base-isolated building under BIGM.

3.4. Influence of Superstructure Characteristics on Performance under Multihazard Scenario. The behavior of base-isolated buildings can be influenced by the characteristics of the superstructure, such as the flexibility and damping of the superstructure. Therefore, the effect of the characteristics of the superstructure on the response of base-isolated buildings is assessed under NF earthquake, FF earthquake, and BIGM considering the bidirectional interaction. The influence of the flexibility of the superstructure is studied by quantifying the different response quantities of base-isolated buildings with different number of stories (N), i.e., 1, 2, 4, 6, and 8 stories. The values of the fundamental time period (T) for the fixed-base models of the buildings with 1, 2, 4, 6, and 8 stories, respectively, are considered as 0.1 s, 0.2 s, 0.4 s, 0.6 s, and 0.8 s, whereas the superstructure damping ratio for all the building models is considered to be 0.05. Five types of base isolation systems, the LRB (T_b = 2.5 s), N-Z system (T_b = 2.5 s, ξ_b = 0.05, and q = 2.5 cm), PF, FPS (T_b = 2.5 s), and R-FBI (T_b = 2.5 s and ξ_b = 0.05), are used to isolate the buildings having different number of stories. The effect of the number of stories on the trends of the resultant top floor

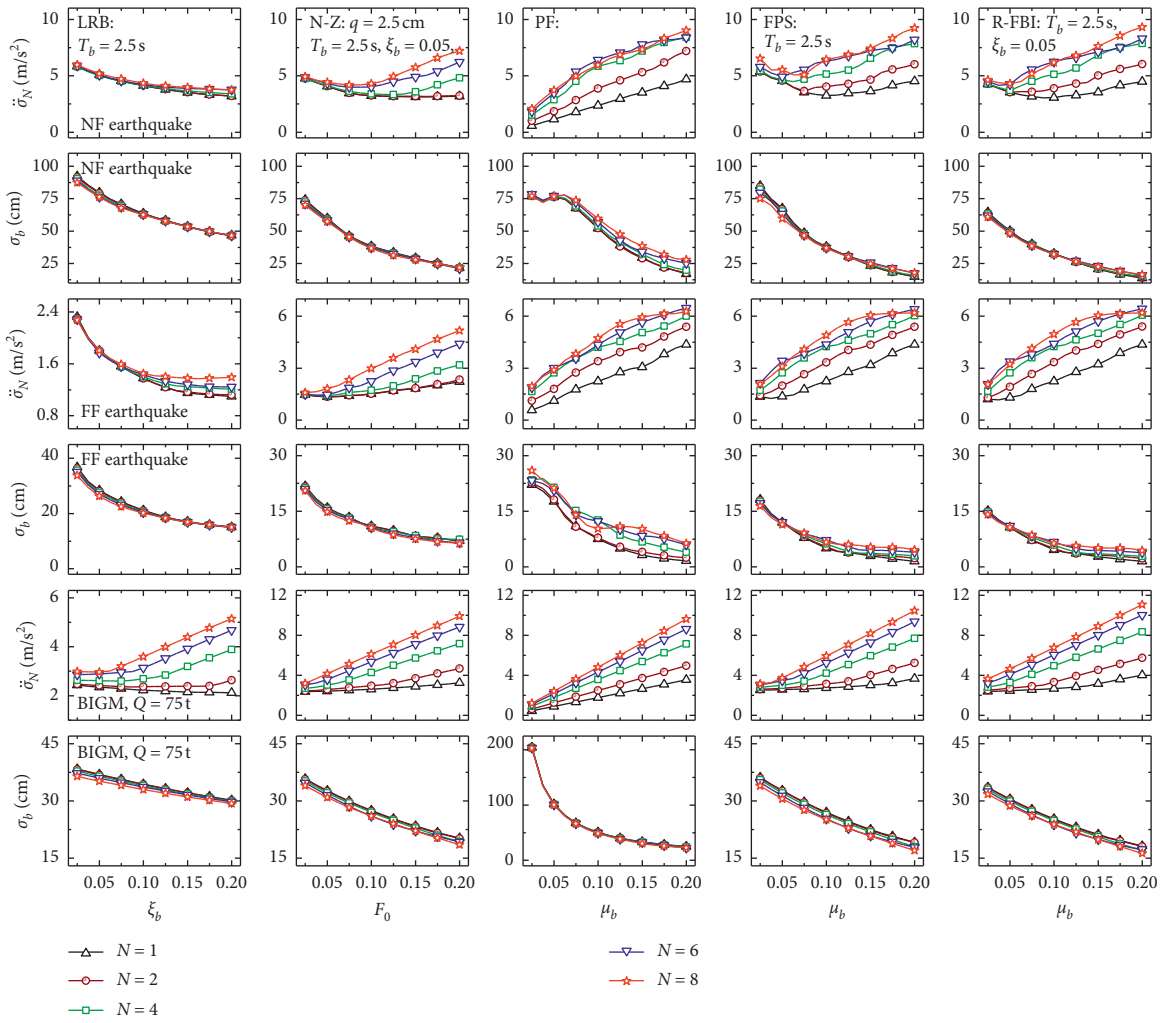

FIGURE 14: The effect of the number of stories on the top floor acceleration and isolator displacement of base-isolated buildings under NF earthquake, FF earthquake, and BIGM.

acceleration and resultant isolator displacement of the base-isolated buildings under NF earthquake, FF earthquake, and BIGM is presented in Figure 14. Under the three types of excitations, the trends of the resultant isolator displacements of the buildings equipped with five base isolators are observed to be identical for buildings having different number of stories. Additionally, similar trends of the resultant top floor acceleration are exhibited by base-isolated buildings having different number of stories. Though, the number of stories of the base-isolated buildings significantly influences the value of the top floor acceleration of the building under NF earthquake, FF earthquake, and BIGM. For all base-isolated buildings under all three types of excitations, the top floor acceleration increases with an increase in the number of stories. Moreover, the influence of the number of stories on the top floor acceleration is found to be prominent for larger values of the damping ratio of LRB, larger values of the normalized yield strength of the N-Z system, and larger values of the friction coefficients of the PF system, FPS, and R-FBI. On the contrary, it is observed that the number of stories of the building typically has less influence on the values of the isolator displacements of the buildings isolated by the LRB, N-Z system, PF system, FPS, and R-FBI under three types of excitations.

The influence of the relative flexibility of the superstructure in X and Y directions is also studied. The ratio of the lateral stiffness of the columns of each story of the building in the Y direction to that of the X direction ($k_{j,Y}/k_{j,X}$) values of 1, 1.2, 1.4, 1.6, and 1.8 is considered. A four-story base-isolated building with a fixed-base fundamental time period of 0.4 s, in the X direction, is studied by using the different values of $k_{j,Y}/k_{j,X}$, under the multihazard scenario of earthquakes (NF earthquake and FF earthquake) and BIGMs. The trends of the resultant top floor acceleration and resultant isolator displacement of four-story base-isolated buildings with different values of $k_{j,Y}/k_{j,X}$ are depicted in Figure 15. The figure shows that the values of the resultant isolator displacements are not influenced significantly by $k_{j,Y}/k_{j,X}$ for the buildings isolated by the LRB, N-Z system, PF system, FPS, and R-FBI under three types of excitations. Also, a larger value of $k_{j,Y}/k_{j,X}$ is observed to result in a reduced value of resultant top floor acceleration, especially

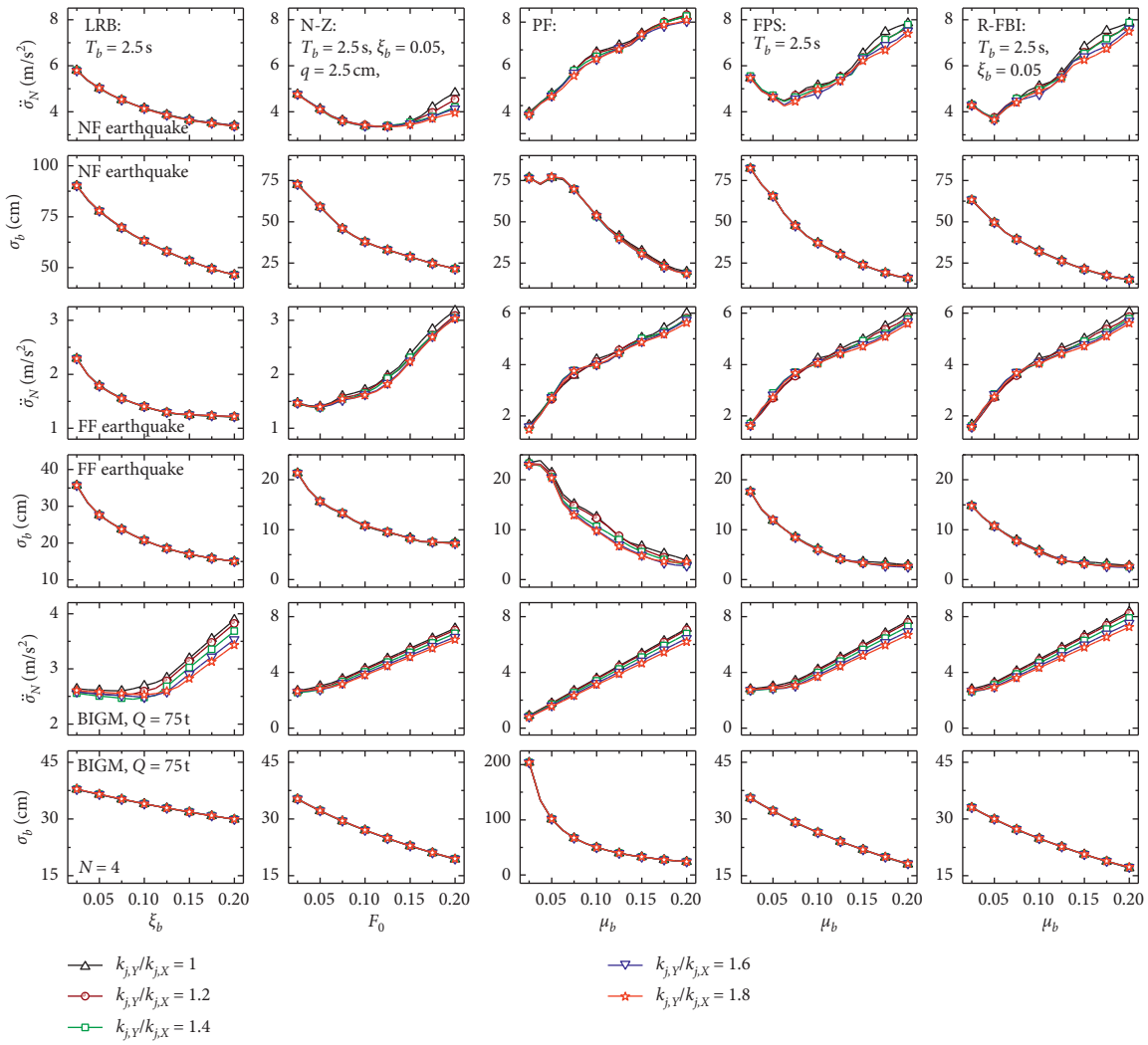

FIGURE 15: The effect of $k_{j,Y}/k_{j,X}$ on the response of four-story base-isolated buildings under NF earthquake, FF earthquake, and BIGM.

for the buildings subjected to BIGM. However, the trends of the resultant top floor acceleration and the resultant isolator displacement obtained for different values of $k_{j,Y}/k_{j,X}$ are the same. Therefore, it can be concluded that the relative flexibility of the superstructure in X and Y directions does not influence the behavior of the symmetrical building under NF earthquakes, FF earthquakes, and BIGMs.

The effect of the damping of the superstructure is evaluated by investigating the response of the four-story base-isolated building considering ξ_s values of 2%, 3.5%, 5%, 6.5%, and 8%. It may be worth mentioning that small structural damping ratio (i.e., 2% or 3.5%) may not be feasible for fixed-base multistory buildings when nonlinear deformation is considered. However, for base-isolated buildings, small values of superstructure damping can reasonably be considered because the superstructure is prominently expected to behave elastically. The resultant top floor acceleration and resultant isolator displacement of the building isolated by the LRB, N-Z system, PF system, FPS, and R-FBI, under NF earthquake, FF earthquake, and BIGM, are obtained, and the trends are plotted in Figure 16. It is observed that superstructure damping does not affect the trends of the resultant top floor acceleration and resultant isolator displacement of the buildings isolated by four base isolation systems. Additionally, it is observed that the superstructure damping ratio does not influence the value of the isolator displacement for the buildings isolated by five base isolation systems under all three types of dynamic base excitations. However, although the trends of the top floor acceleration are the same, the results presented in Figure 16 show that a larger superstructure damping ratio typically results in a smaller value of top floor

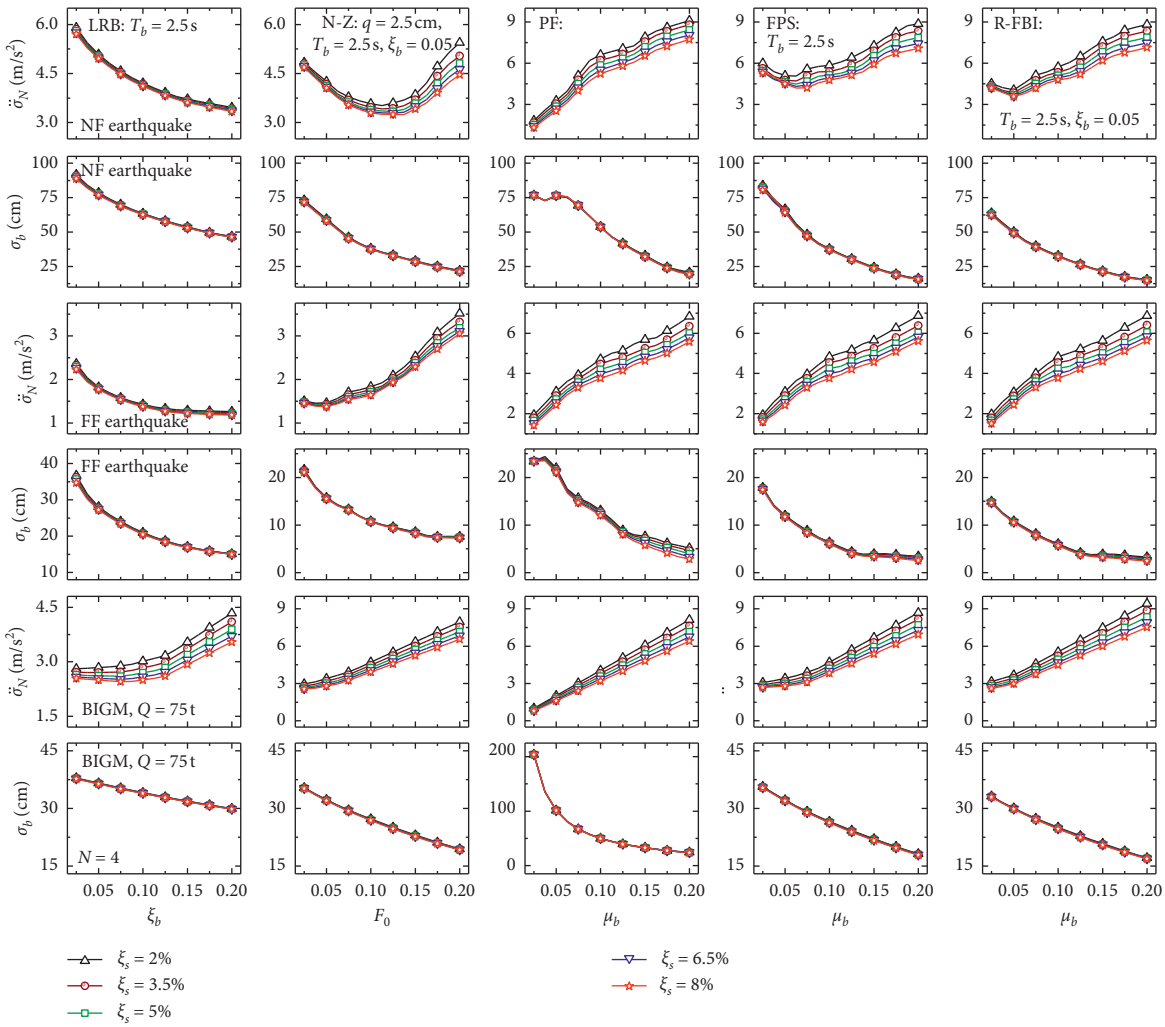

Figure 16: The effect of the superstructure damping on the response of the four-story base-isolated buildings under NF earthquake, FF earthquake, and BIGM.

acceleration. Therefore, based on the observations, it can be concluded that the superstructure characteristics have less influence on the behavior of the base-isolated buildings under the multihazard loading scenario of earthquakes (NF earthquakes and FF earthquakes) and BIGMs, as compared to the properties of the base isolators.

4. Conclusions

This study presents an investigation of the behavior of multistory buildings isolated by various types of elastomeric and sliding base isolation systems under multihazard loading. The multihazard scenario of earthquakes (near-fault and far-fault earthquake) and blast-induced ground motion (BIGM) is considered, wherein the bidirectional effects of the hazards are taken into account. The influence of the selection of different values of the parameters of isolators on the key response quantities of the buildings, such as the top floor acceleration, top floor displacement, isolator displacement, base shear, interstory drift ratio, and total superstructure drift ratio, are assessed under the multihazard scenario. Furthermore, the influence of the properties of the superstructure (superstructure flexibility and superstructure damping ratio) on the behavior of the base-isolated buildings under multihazard loading is assessed. Based on the findings of the extensive numerical studies, it is concluded that base-isolated buildings behave differently under the near-fault earthquake, far-fault earthquake, and blast-induced ground motion. Consequently, the design of the isolation systems and the selection of suitable parameters thereof shall be done cautiously, accounting for the effects of both types of hazards considered on the buildings. The specific conclusions of the study are listed as follows:

(1) Although the base isolation technology can help in protecting buildings from three types of dynamic base excitations (NF earthquakes, FF earthquakes, and BIGMs), the base-isolated buildings behave differently under different multiple hazards.

(2) The response quantities of the base-isolated buildings obtained with and without the consideration of bidirectional interaction are significantly different. The resultant isolator displacement is

underestimated, and the resultant top floor acceleration and resultant base shear are overestimated when the bidirectional interaction is neglected.

(3) For the building isolated by LRB, an increase in ξ_b results in the reduction of all the six response quantities of the building under NF and FF earthquakes. However, the acceleration response increases with ξ_b for the building subjected to BIGM.

(4) For the N-Z system, an increase in F_0 results in an initial reduction followed by an increase in the top floor acceleration, base shear, interstory drift, and total superstructure drift of the base-isolated building under NF earthquakes. On the contrary, all the four response quantities consistently increase with F_0 for BIGM.

(5) The trends of the response quantities of the building isolated by the PF system observed under NF earthquakes, FF earthquakes, and BIGMs are similar.

(6) For the buildings isolated by the FPS and R-FBI, the trends of the top floor displacement and the isolator displacement show a reducing trend for an increase in the value of μ_b under NF earthquakes, FF earthquakes, and BIGMs. However, the influence of the friction coefficient of the FPS on the trends of the top floor acceleration, base shear, interstory drift, and total superstructure drift is different for the three types of excitations.

(7) Under NF earthquakes, FF earthquakes, and BIGMs, the trends of the top floor acceleration and the isolator displacement are similar for the base-isolated buildings with different number of stories (i.e., $N = 1, 2, 4, 6, 8$). Furthermore, the relative flexibility of the superstructure in X and Y directions does not influence the behavior of the building for all three types of dynamic base excitations, NF earthquakes, FF earthquakes, and BIGMs.

(8) Superstructure damping does not influence the trends of the top floor acceleration and the isolator displacement under NF earthquakes, FF earthquakes, and BIGMs, for the considered range of isolator parameters.

(9) The behavior of base-isolated buildings, under multihazard loading scenario of earthquakes and BIGMs, is influenced more by the properties of base isolators as compared to that of the superstructure.

Data Availability

The data used to support the findings of this study are available from the corresponding author upon request.

Conflicts of Interest

The authors declare that they have no conflicts of interest.

References

[1] V. A. Zayas, S. S. Low, and S. A. Mahin, "A simple pendulum technique for achieving seismic isolation," *Earthquake Spectra*, vol. 6, no. 2, pp. 317–333, 1990.

[2] T. T. Soong and B. F. Spencer Jr., "Active, semi-active and hybrid control of structures," in *Proceedings of the Twelfth World Conference on Earthquake Engineering*, Auckland, New Zealand, February 2000.

[3] M. H. Stanikzai, S. Elias, V. A. Matsagar, and A. K. Jain, "Seismic response control of base-isolated buildings using multiple tuned mass dampers," *The Structural Design Of Tall And Special Buildings*, vol. 28, p. e1576, 2018.

[4] R. Rupakhety, S. Elias, and S. Olafsson, "Shared tuned mass dampers for mitigation of seismic pounding," *Applied Sciences*, vol. 10, no. 6, p. 1918, 2020.

[5] J. M. Kelly, "Aseismic base isolation: review and bibliography," *Soil Dynamics and Earthquake Engineering*, vol. 5, no. 3, pp. 202–216, 1986.

[6] R. S. Jangid and T. K. Datta, "Seismic behaviour of base-isolated buildings: a state-of-the art review," *inProceedings of the Institution of Civil Engineers-Structures and Buildings*, vol. 110, no. 2, pp. 186–203, 1995.

[7] C.-M. Chang and B. F. Spencer, "Active base isolation of buildings subjected to seismic excitations," *Earthquake Engineering & Structural Dynamics*, vol. 39, no. 13, pp. 1493–1512, 2010.

[8] Y. Peng, L. Ding, and J. Chen, "Performance evaluation of base-isolated structures with sliding hydromagnetic bearings," *Structural Control and Health Monitoring*, vol. 26, no. 1, p. e2278, 2018.

[9] R. Rabiee and Y. Chae, "Adaptive base isolation system to achieve structural resiliency under both short- and long-period earthquake ground motions," *Journal of Intelligent Material Systems and Structures*, vol. 30, no. 1, pp. 16–31, 2018.

[10] Y. Peng and T. Huang, "Sliding implant-magnetic bearing for adaptive seismic mitigation of base-isolated structures," *Structural Control and Health Monitoring*, vol. 26, no. 10, 2019.

[11] P. Gardoni, C. Murphy, and A. Rowell, *Risk Analysis of Natural Hazards: Interdisciplinary Challenges and Integrated Solutions*, Springer, Berlin, Germany, 2016.

[12] P. Gardoni and J. M. LaFave, *Multi-Hazard Approaches to Civil Infrastructure Engineering*, Springer, Berlin, Germany, 2016.

[13] T. B. Messervey, D. Zangani, and S. Casciati, "Smart high-performance materials for the multi-hazard protection of civil infrastructure," *Safety And Security Engineering III*, vol. 108, 2009.

[14] H. Mahmoud and A. Chulahwat, "Multi-hazard multi-objective optimization of building systems with isolated floors under seismic and wind demands," In P. Gardoni, J. LaFave. (eds) Multi-hazard Approaches to Civil Infrastructure Engineering. Springer, Cham, Switzerland, 2016.

[15] I. Venanzi, O. Lavan, L. Ierimonti, and S. Fabrizi, "Multi-hazard loss analysis of tall buildings under wind and seismic loads," *Structure and Infrastructure Engineering*, vol. 14, no. 10, pp. 1295–1311, 2018.

[16] T. Roy and V. Matsagar, "Effectiveness of passive response control devices in buildings under earthquake and wind during design life," *Structure and Infrastructure Engineering*, vol. 15, no. 2, pp. 252–268, 2019.

[17] T. Roy and V. Matsagar, "Probabilistic assessment of steel buildings installed with passive control devices under multi-hazard scenario of earthquake and wind," *Structural Safety*, vol. 85, p. 101955, 2020.

[18] P. Henderson and M. Novak, "Response of base-isolated buildings to wind loading," *Earthquake Engineering & Structural Dynamics*, vol. 18, no. 8, pp. 1201–1217, 1989.

[19] P. Henderson and M. Novak, "Wind effects on base isolated buildings," *Journal of Wind Engineering and Industrial Aerodynamics*, vol. 36, no. 1–3, pp. 559–569, 1990.

[20] Y. Chen and G. Ahmadi, "Wind effects on base-isolated structures," *Journal of Engineering Mechanics*, vol. 118, no. 8, pp. 1708–1727, 1992.

[21] A. Kareem, "Modelling of base-isolated buildings with passive dampers under winds," *Journal of Wind Engineering and Industrial Aerodynamics*, vol. 72, pp. 323–333, 1997.

[22] B. Liang, X. Shishu, and T. Jiaxiang, "Wind effects on habitability of base-isolated buildings," *Journal of Wind Engineering and Industrial Aerodynamics*, vol. 90, no. 12–15, pp. 1951–1958, 2002.

[23] C. Feng and X. Chen, "Evaluation and characterization of probabilistic alongwind and crosswind responses of base-isolated tall buildings," *Journal of Engineering Mechanics*, vol. 145, no. 12, Article ID 04019097, 2019.

[24] R. Zhang and B. M. Phillips, "Numerical study on the benefits of base isolation for blast loading," in *Joint 6th International Conference on Advances in Experimental Structural Engineering (6AESE) and 11th International Workshop on Advanced Smart Materials and Smart Structures Technology (11ANCRiSST)*, Champaign, IL, USA, August 2015.

[25] R. Zhang and B. M. Phillips, "Performance and protection of base-isolated structures under blast loading," *Journal of Engineering Mechanics*, vol. 142, no. 1, Article ID 04015063, 2016.

[26] M. Z. Kangda and S. Bakre, "Positive-phase blast effects on base-isolated structures," *Arabian Journal for Science and Engineering*, vol. 44, no. 5, pp. 4971–4992, 2018.

[27] P. D. Mondal, A. D. Ghosh, and S. Chakraborty, "Performance of N-Z base isolation system for structures subject to underground blast," *inProceedings Of the International Symposium On Engineering under Uncertainty: Safety Assessment And Management (ISEUSAM-2012)*, Springer, Berlin, Germany, pp. 1007–1020, 2012.

[28] P. D. Mondal, A. D. Ghosh, and S. Chakraborty, "Performance of N-Z systems in the mitigation of underground blast induced vibration of structures," *Journal of Vibration and Control*, vol. 20, no. 13, pp. 2019–2031, 2013.

[29] P. D. Mondal, A. D. Ghosh, and S. Chakraborty, "Control of underground blast-induced building vibration by shape-memory-alloy rubber bearing (SMARB)," *Structural Control and Health Monitoring*, vol. 24, no. 10, p. e1983, 2017.

[30] P. D. Mondal, A. D. Ghosh, and S. Chakraborty, "Performances of various base isolation systems in mitigation of structural vibration due to underground blast induced ground motion," *International Journal of Structural Stability and Dynamics*, vol. 17, no. 4, p. 1750043, 2017.

[31] J. P. Talbot and H. E. M. Hunt, "Isolation of buildings from rail-tunnel vibration: a review," *Building Acoustics*, vol. 10, no. 3, pp. 177–192, 2003.

[32] L. S. Wei and F. L. Zhou, "Vibration and seismic isolation design for buildings on subway platform," in *Proceedings of the Fourteenth World Conference on Earthquake Engineering*, Beijing, China, October 2008.

[33] D. Makovicka and D. Makovicka, "Structure isolation in order to reduce vibration transfer from the subsoil," *International Journal of Computational Methods and Experimental Measurements*, vol. 2, no. 1, pp. 1–13, 2014.

[34] Y. K. Wen, "Method for random vibrations of hysteretic systems," *Journal of the Engineering Mechanics Division*, vol. 102, no. 2, pp. 249–263, 1976.

[35] Y. K. Wen, "Methods of random vibration for inelastic structures," *Applied Mechanics Reviews*, vol. 42, no. 2, pp. 39–52, 1989.

[36] Y. J. Park, Y. K. Wen, and A. H.-S. Ang, "Random vibration of hysteretic systems under Bi-directional ground motions," *Earthquake Engineering & Structural Dynamics*, vol. 14, no. 4, pp. 543–557, 1986.

[37] V. A. Matsagar and R. S. Jangid, "Viscoelastic damper connected to adjacent structures involving seismic isolation," *Journal of Civil Engineering and Management*, vol. 11, no. 4, pp. 309–322, 2005.

[38] R. S. Jangid, "Computational numerical models for seismic response of structures isolated by sliding systems," *Structural Control and Health Monitoring*, vol. 12, no. 1, pp. 117–137, 2005.

[39] R. S. Jangid, "Optimum lead-rubber isolation bearings for near-fault motions," *Engineering Structures*, vol. 29, no. 10, pp. 2503–2513, 2007.

[40] E. M. L. Carvalho and R. C. Battista, "Blast-induced vibrations in urban residential buildings," *inProceedings of the Institution of Civil Engineers-Structures and Buildings*, vol. 156, no. 3, pp. 243–253, 2003.

[41] C. Wu and H. Hao, "Numerical study of characteristics of underground blast induced surface ground motion and their effect on above-ground structures. Part I. Ground motion characteristics," *Soil Dynamics and Earthquake Engineering*, vol. 25, no. 1, pp. 39–53, 2005.